



Process optimization and mathematical modelling of photo-fermentative hydrogen production from dark fermentative cheese whey effluent by *Rhodobacter sphaeroides* O.U.001 in 2-L cylindrical bioreactor

Raman Rao¹ · Nitai Basak¹

Received: 18 December 2020 / Revised: 10 February 2021 / Accepted: 11 February 2021 / Published online: 23 February 2021
© The Author(s), under exclusive licence to Springer-Verlag GmbH, DE part of Springer Nature 2021

Abstract

In this study, organic acids present in dark fermentative cheese whey effluent (DFCWE) were utilized to produce biological hydrogen via photo fermentation by *R. sphaeroides* O.U.001 cells in 2-L double-walled cylindrical PBR with a working volume of 1.5 L. Plackett-Burman design-based analysis revealed organic acid concentration (OA), temperature, and light intensity as the most significant variables. Experiments were performed at different conditions of (OA, 8–16 g L⁻¹), temperature (25–37 °C), and light intensity (8–12 klx). Optimum values were obtained by Box-Behnken design matrix (BBD) based on the impact on hydrogen production rate (HPR) and under optimum values (OA concentration, 12 g L⁻¹; temperature, 31 °C; and light intensity, 10 klx); HPR of 41.94 mL L⁻¹ h⁻¹ was obtained, which lies in close proximity with the predicted production rate of 41.65 mL L⁻¹ h⁻¹ with the correlation coefficient (R^2) and coefficient of variance as 0.9801 and 0.0521, respectively. PBR performance for treating DFCWE was checked by performing mathematical modelling using four models. Kinetic study of DFCWE consumption and growth profile of the bacterial cell were investigated by fitting experimental values into Monod and logistic equations, respectively. Parameters of the modified Gompertz equation and Luedeking-Piret models gave proper simulated fitting with experimental H₂ production obtained under optimized bioprocess variables. Metabolite analysis revealed that acetic and lactic acids were utilized to produce biohydrogen under uncontrolled pH. Findings of the current investigation could be a promising strategy for obtaining better hydrogen productivity in photo fermentation.

Keywords Cheese whey effluent · Photo fermentation · Photobioreactor · Box-Behnken design · Hydrogen production rate · Kinetic study

Highlights

- Batch hydrogen production from dark fermentative cheese whey effluent in 2-L double-walled cylindrical photobioreactor;
- Total organic acid concentration, temperature, and light intensity affect hydrogen production rate;
- Fermentation experiment was designed using Box-Behnken design of RSM;
- Optimal hydrogen production rate was 41.65 mL L⁻¹ h⁻¹ at total organic acid concentration of 12 g L⁻¹, temperature 31 °C, and light intensity 10 klx;
- Modelling of photo fermentation by unstructured models at statistically optimized variables gave satisfactory fitting with experimental data;
- Statistical and mathematical modelling of biohydrogen production may provide useful insights for waste to hydrogen endeavors.

✉ Nitai Basak
basakn@nitj.ac.in; basakn812@yahoo.com

¹ Department of Biotechnology, Dr. B R Ambedkar National Institute of Technology Jalandhar, Jalandhar 144011, India

1 Introduction

Microbial production of hydrogen (H₂) has been used extensively by the research fraternity around the globe as a suitable alternative to thermochemical-based methods for generating H₂ gas equivalent to fuel grade [1, 2]. These methods can be broadly divided into two main categories: algal- and cyanobacteria-based biophotolysis of water and fermentative route using organic compounds either in the absence (dark fermentation, DF) or in the presence of light source (photo fermentation, PF) [3–5]. Fermentative H₂ production could occur at different temperatures, from the psychrophilic to thermophilic ranges [6, 7], and is based on the utilization of cheap and abundant renewable organic feedstock [8]. Significant research in this area has been reported earlier [4, 9–11]. Depending upon the metabolic activity of H₂-producing

bacteria during DF, the main volatile fatty acids (VFAs) reported are acetate and butyrate along with lactate, propionate, and ethanol [12]. These metabolites, if not recovered, inhibit the growth of H₂-producing bacteria, and as a result, the H₂ yield is lowered. In order to improve the yield, the VFAs can be further utilized as a low-cost potential feedstock (after pre-treatment if required) in other bioprocesses such as in PF, electricity production in microbial fuel cell, methanogenesis, and electrohydrogenesis for H₂ production [13]. In this context, sequential dark-photo fermentation is a salient approach which has the potential to overcome the limitations of lower H₂ yield of single-step DF and PF. The mixture of gases containing carbon dioxide and hydrogen, stored in the head space of a bioreactor during DF, is collected and purified. The left-over acids present in the spent media of DF (Eq. 1) is then fed to another bioreactor in second-stage PF (Eq. 2) after certain adjustments in terms of composition of VFAs, pH, and filtration/centrifugation to remove any dark fermentative bacterial cell debris. Subsequent PF is mediated by various photosynthetic bacteria such as purple nonsulfur bacteria (PNS) at a high degradation rate as compared to DF [14].



Requirement of two separate bioreactors in sequential fermentation has an advantage in that optimization in operating parameters for each fermentation process can be done independently, which could enhance the overall biohydrogen yield. Integration of DF and PF can yield up to 12 mol of H₂ per mol of glucose and could be an ideal blueprint for deriving additional H₂ [15]. Specialized literature showed that *Rhodobacter sphaeroides* O.U.001 were able to ferment acetate, butyrate, and lactate as the sole source of carbon (either individually or in mixture form) to produce H₂ [16]. The process occurs under anoxygenic conditions and requires optimum light intensity, coming from either natural (in outdoor conditions) or artificial sources of light (tungsten bulb, LED lights, etc. in indoor environment). On a theoretical basis, the complete photo conversion of commonly used organic acids into H₂ by PNS bacteria is shown in Table 1 [17]. It is evident that malic and lactic acids are the most preferable substrates having a positive effect on the biohydrogen production rate. The organic acids shown in Table 1 are generally found in the waste stream of food processing industries and can be utilized positively by PNS bacterial cells for H₂ production.

PF has the advantage that produced biogas is significantly pure and contains H₂ content equivalent to 80% [18]. The PNS microbial cells such as *R. sphaeroides* O.U.001, *R. sphaeroides*-RV, and *Rhodospseudomonas palustris* are prominent in oxidizing the different organic acids which are present in enormous quantity in the dark fermentative waste

Table 1 Theoretical photo-fermentative biohydrogen yield using different carbon source

C ₄ H ₆ O ₅ (malic acid)+3H ₂ O	→6H ₂ +4CO ₂
C ₂ H ₄ O ₂ (acetic acid)+2H ₂ O	→4H ₂ +2CO ₂
C ₂ H ₄ O ₂ (acetic acid)+2H ₂ O	→4H ₂ +2CO ₂
C ₄ H ₈ O ₂ (butyric acid)+6H ₂ O	→10H ₂ +4CO ₂
C ₃ H ₆ O ₃ (lactic acid)+3H ₂ O	→6H ₂ +3CO ₂

stream via adenosine triphosphate (ATP)-dependent biochemical reaction [13, 19, 20]. These acids include malic acid, acetic acid, butyric acid, lactic acid, propionic acid, and up to a lesser extent succinic acid also. Utilization of these acids in the PBR towards effective H₂ generation depends upon operating conditions viz. substrate concentration, fermentative temperature, pH, inoculum age of PNS bacteria, light source, and illumination intensity [10, 21, 22]. The main hurdle encountered during PF process is to improve the H₂ yield and HPR, which can be achieved by optimizing as many culture variables as possible. Response surface methodology (RSM) has been used in recent times to optimize photo-fermentative H₂ yield in batch mode [23–27]. OA concentration is an important parameter during PF because an excess of substrate concentration may increase the viscosity of fermentation media, which in turn disturbs the mass transfer of substrate towards bacterial cells and H₂ production is inhibited [28]. Different operating parameters such as pH, fermentation time, and temperature are known to govern the stability of fermentative H₂ production system and composition of OA [29]. pH regulates the metabolic activity and H₂ production capability of microbes since various physiological parameters such as membrane potential and proton motive force of the cells are dependent upon the change in external pH [30]. Another important operating parameter is temperature which affects the H₂-producing potential of PNS cells. Any fluctuation in the optimum temperature range (30–35 °C) of PNS bacteria negatively affects the HPR and H₂ yield [31]. The growth of PNS bacteria starts at a minimum threshold value of light intensity, followed by increase in HPR with increase in light intensity. Maximum growth happens at an optimum level, then the saturation effect decreases the growth rate due to excess of ATP and FD_{red}. Different species among PNS require different light intensities to grow and produce H₂ effectively due to variation in their photo-adaptation capability [32]. Therefore, in order to maximize the productivity of H₂, it becomes necessary to optimize the light intensity.

During literature survey, we observed that most studies involve the optimization of simple acids by using a statistical tool [24, 33–36]. But statistical optimization of OA concentration present in dark fermentative spent media has not been much explored. Mishra et al. [37] applied BBD to determine the effect of dark fermented palm oil effluent concentration,

light intensity, and agitation rate on biohydrogen production by using *R. palustris* cells. Similarly, Uyar et al. [16] used a mixture of volatile acids (malic, acetic, butyric, lactic, and propionic acid) present in dark fermentation liquor for photo-fermentative H₂ generation by *R. sphaeroides* O.U.001 cells, but optimization of operative parameters was not performed. Although, significant work has been done in utilizing spent media of DF for the subsequent PF process (either in a sequential manner in two different reactors or by combined fermentation in a single reactor) to improve H₂ yield [4, 38–40]. CW has also been explored for producing biohydrogen via both DF [9, 41–43] and PF [42, 44] processes. Rai et al. [45] have used spent media of dark fermented CW wastewater (containing mainly acetic and butyric acid) as the PF substrate for producing biohydrogen by *R. palustris* BHU 01 cells, but the optimization of concentration of OA along with temperature and illumination intensity was missing in this communication.

The complexity of the metabolic pathway adopted by PNS bacteria and its growth characteristics during photo-fermentative H₂ production can be better understood by applying unstructured mathematical models. These models help in interpretation/integration of the experimental data of H₂ production and provide more in-depth understanding of the complex fermentation system [46]. Mathematical tools demonstrate the important processes inside the PBR such as pH, temperature, feedstock degradation, and biomass growth and also assist in acquiring knowledge for building efficient PBR for H₂ production [47]. In this context, researchers around the globe have put forward different mathematical models to explain the fermentation behavior during H₂ production [48, 49]. But only few studies have done the kinetic analysis of biohydrogen production in terms of microbial growth, formation of product, and consumption of substrate under optimized engineering parameters [46, 50]. After reviewing the literature, it was observed that most of the kinetic studies on biohydrogen production system have been done in the case of a dark fermentative system, and very limited number of publications is available related to mathematical modelling of photo-fermentative H₂ production under statistically optimized operating conditions. Use of an unstructured kinetic model for determining the behavior of the PF system as a function of the fate of sugar containing waste effluent as a substrate, growth of photo-fermentative bacteria, and product formation has not been explored much to date. The present study tried to fill this void for modelling the photo-fermentative microbial system with the help of four well-known kinetic models, namely, the Monod model, logistic model, modified Gompertz equation, and Luedeking-Piret model. An attempt was made to study the kinetics of batch H₂ fermentation in 2-L cylindrical PBR under optimized conditions of bioprocess variables.

Monitoring of cell growth profile of *R. sphaeroides* O.U.001 during PF has been investigated on the basis of a logistic model. Use of a logistic model in the current study was attributed to the fact that it has the additional advantage of representing the entire growth curve, including the lag phase, the exponential growth, and the stationary phases [47, 51], and takes into account growth inhibition in the stationary phase of growth as well. Expression of substrate utilization kinetics (consumption of DFCWE) by *R. sphaeroides* O.U.001 was obtained by applying the Monod model. Further, to analyze the profile of H₂ formation during batch fermentation, modified Gompertz equation, and Luedeking-Piret model were applied. Validation of these mathematical models was done by comparing with the observed data of H₂ production under optimized conditions. The value of kinetic parameters of the logistic fit model (apparent specific growth rate, K_c in h; maximum biomass concentration, X_{max} in g dry weight L⁻¹ and $1 - X_0/X_{max}$), modified Gompertz equation (maximum cumulative H₂ produced, $P_{max,i}$ in mL; maximum rate of H₂ production, R_{max} in mL L⁻¹ h⁻¹; lag time of bacteria, λ in h) were obtained by non-linear curve fitting of the mathematical models with the experimental data during batch PF. The outcome of mathematical modelling based on lab scale data will significantly help the researchers around the globe in scaling up the batch PF process by giving useful information related to designing of the PBR, analysis of microbial behavior of PNS bacteria, relation between H₂ production and growth rate of H₂ producing bacterial cell, etc.

In view of the above, it was observed that to the best of the authors' knowledge, statistical optimization of OA concentration, temperature, and light intensity in the subsequent second stage of the DFCWE-based PF system followed by its mathematical kinetic studies has not been pointed out till now. Additional novelty of the present work towards photo-fermentative biohydrogen production is also provided by the fabrication of a 2-L prototype form of commercial PBR. It resembled with the commercial bioreactors in having a cylindrical shape, magnetic stirrer-based agitation, and presence of a double chamber along with various ports. Given the limited number of reported studies related to the mathematical modelling of a PF system at optimum conditions, the present communication is believed to open the path for further research for the economical production of biohydrogen and has the following two objectives based on the analysis of the research gap in the area of PF: (1) study of individual and interactive effects of OA concentration, temperature, and light intensity on HPR using 3K BBD matrix from DFCWE in 1.5-L fermentation volume by growing cells of *R. sphaeroides* O.U.001; (2) use of fermentation models to understand the behavior of DFCWE-based photo-fermentative H₂ production system in batch mode.

2 Materials and methods

2.1 Microorganism and culture conditions

R. sphaeroides O.U.001 cells (from the Department of Biotechnology, Indian Institute of Technology, Kharagpur, India) were used as source of inoculum for PF and were cultivated photo-heterotrophically in modified Biebl and Pfenning's media containing DL malic acid 1.0 g L^{-1} and glutamic acid 1.48 g L^{-1} [52]. Cells were grown in 100 mL of media with initial pH adjusted to 6.8 ± 0.2 , and the flask was incubated at $32 \pm 2 \text{ }^\circ\text{C}$ in anaerobic conditions. Uniform light distribution of 8–10 klx was achieved by placing a Philips LED bulb (60 W). Periodic sparging of argon gas (99.99% purity) was done in the flask to maintain anaerobic conditions. Cells were preserved in the anaerobic environment as the stabbed culture in nutrient agar. Further gram staining and microscopic observation was done to ensure the purity of *R. sphaeroides* cells, and suspension culture was generated by picking a single colony of bacterial cells.

For initializing biohydrogen production, 48-h-old *R. sphaeroides* O.U. 001 cells fully grown on modified Biebl and Pfenning's media were centrifuged at 6000 rpm for 20 min, and collected cells were transferred to media containing DFCWE with the following composition (per liter): glutamic acid 0.3 g; NaCl 0.4 g; yeast extract 0.4 g; $\text{MgSO}_4 \cdot 7\text{H}_2\text{O}$ 0.2 g; KH_2PO_4 0.5 g; $\text{CaCl}_2 \cdot 2\text{H}_2\text{O}$ 0.05 g; ferric citrate 5 mL; and trace element solution 1 mL (having in mg L^{-1} : ZnCl_2 60; H_3BO_3 60; $\text{MnCl}_2 \cdot 4\text{H}_2\text{O}$ 100; $\text{CoCl}_2 \cdot 6\text{H}_2\text{O}$ 200, $\text{CuCl}_2 \cdot 2\text{H}_2\text{O}$ 20;

$\text{NiCl}_2 \cdot 6\text{H}_2\text{O}$ 20; $(\text{NH}_4)_2\text{MoO}_4 \cdot 2\text{H}_2\text{O}$ 40; and HCl (25 % v/v) 1 mL L^{-1}). Preadaptation of bacterial cells in DFCWE was repeated three times by transferring into fresh media to acclimatize bacterial cells with production media, towards maximum H_2 production.

2.2 Set-up of double-walled 2-L cylindrical PBR

The PBR was constructed from glass material (with height 280 mm, outer diameter without water jacket 93 mm, and thickness of 12 mm) having fermentation volume of 1.5 L. Figure 1 depicts the design of PBR used along with its associated set-up. The PBR was fitted with mainly three ports: one for monitoring temperature during fermentation, one port for sparging argon gas, and another port for collecting evolved gas during fermentation. Uniform temperature was maintained by connecting the outer jacket of PBR with a circulatory water bath (Julabo ME F33). Mixing between *R. sphaeroides* cells and substrate inside PBR was achieved by stirring the production media at 200 rpm by a magnetic stirrer (Tarson). Sample to determine bacterial cell density, residual organic acid concentration, and pH during PF was collected at regular intervals of time from the designated sampling port attached to the outer layer of PBR, under aseptic conditions. Produced gases from PBR were collected by downward displacement of 5% (w/v) $\text{K}_2\text{Cr}_2\text{O}_7$ solution at ambient temperature and pressure after passing the gas stream through 50 mL of 7 M KOH solution to remove CO_2 traces from the gaseous mixture.

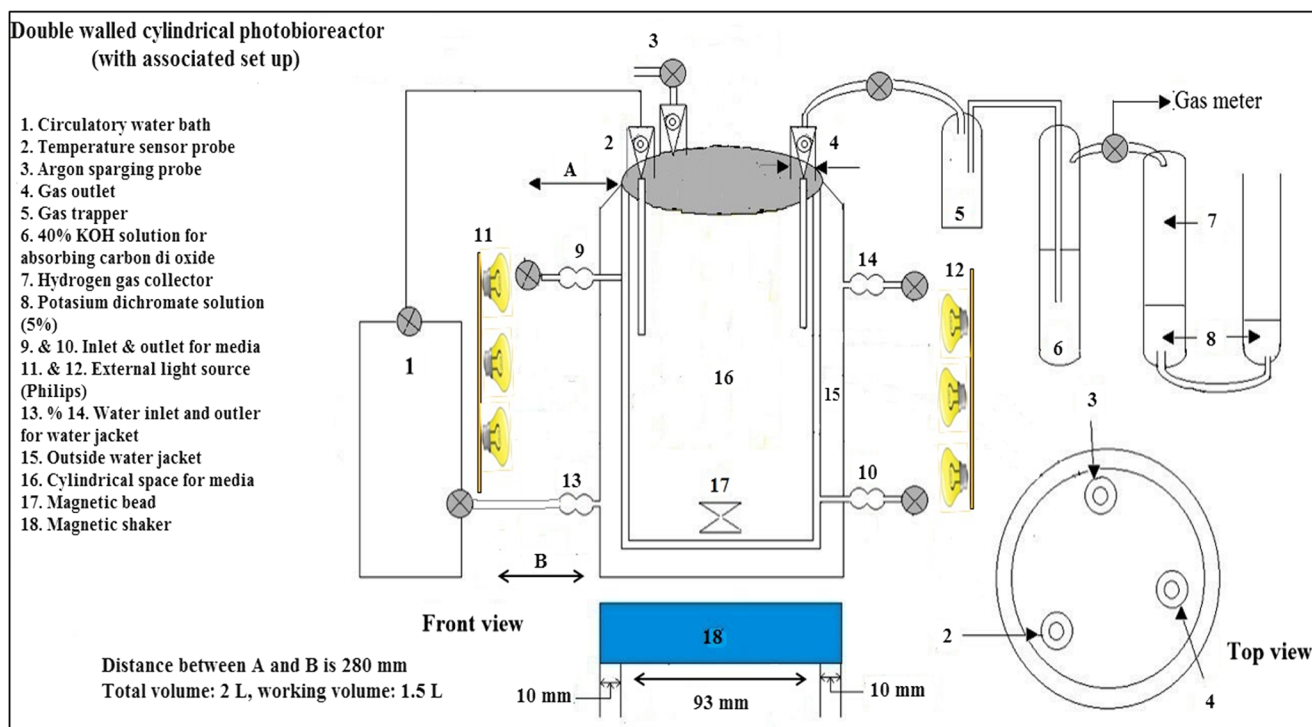


Fig. 1 Schematic design of fermenter-type cylindrical PBR used for biohydrogen production by *R. sphaeroides* O.U.001 cells in batch mode

2.3 DFCWE generation and its subsequent PF

Fresh CW was collected from a local dairy industry in Jalandhar, India. It had carbon content, total carbohydrate content (measured after autoclaving), and lactic acid concentration of 46.72% (w/w), $47.5 \pm 2.0 \text{ g L}^{-1}$, and $0.45 \pm 0.05 \text{ g L}^{-1}$, respectively. Fermentation media contained fresh raw cheese whey having a concentration of $32.5 \text{ g lactose L}^{-1}$ and was supplemented with beef extract 0.75 g L^{-1} , yeast extract 1.5 g L^{-1} , peptone 7.5 g L^{-1} , and NaCl 0.75 g L^{-1} . Fermentation was carried out at a working volume of 1 L, and inoculation was done into the bioreactor with 10% (v/v) of *E. aerogenes* 2822 free cells, harvested at the exponential phase at $31 \pm 2 \text{ }^\circ\text{C}$ and 200 rpm. Anaerobic conditions inside the bioreactor were maintained by flushing the nitrogen gas for 10 minutes. Initially, pH was adjusted to 6.8 ± 0.2 by 0.5 N NaOH solutions. The pH of fermentation media was not controlled during the operation.

DFCWE obtained after dark fermentation was centrifuged at 1000 rpm for 20 minutes to remove any colloidal particles that may inhibit light penetration. After centrifugation, the supernatant was filtered through a 0.22-micron cellulose membrane to remove any suspended particles from the media. It was sterilized at $121 \text{ }^\circ\text{C}$ and steam pressure of 1.05 kg cm^{-2} for 15 minutes. The supernatant obtained after the centrifugation was stored in a deep fridge at $4 \text{ }^\circ\text{C}$, and it was replenished with the fresh sample if any sign of acidification was shown.

DFCWE had major fraction of acetic and lactic acids with some fraction of formic acid and butyric acid and exhibited high concentration of organic acid equivalent to 10 g L^{-1} (120 mM) out of which concentration of acetic acid and lactic acid was $2.5 \pm 0.1 \text{ g L}^{-1}$ ($40 \text{ mM} \pm 1 \text{ mM}$) and $7.5 \pm 0.1 \text{ g L}^{-1}$ ($80 \text{ mM} \pm 1 \text{ mM}$), respectively. Before PF, bacterial cells were pre-activated by growing on DFCWE media in order to make the cells capable of growing in different organic acids present in DFCWE. After 216 h of adaptation, *R. sphaeroides* cells showed improved growth. Production media contained same strength of micronutrients as required for routine growth of PNS bacteria except the carbon source. The medium was inoculated with 10% (v/v) of 24-h-old *R. sphaeroides* cells, and fermentation was carried out at 1.5 L of working volume in an anaerobic condition. The bacterial cells were illuminated with multiple external light sources, i.e., Philips CFL bulb (23 W) and LED bulb (60 W). Overall light intensity of 8–10 klx was maintained by placing three packs of each LED and CFL bulbs at a distance of 25 cm from the surface of PBR. The initial pH of the fermentation medium was controlled by using 1.0 N of NaOH solutions. Concentration of biohydrogen, production rate, and pH were regularly measured over the total duration of the batch fermentation. Each batch test was performed in triplicates with the same source of CW, and results were expressed with a range of standard deviation within 5% to get reproducible results.

2.4 Analytical methods

Bacterial cell population in PBR was measured with the help of a UV-Vis spectrophotometer (Eppendorf BioSpectrometer Kinetic, USA) at 600 nm and path length of 10 mm. The value of pH was observed with the help of a glass electrode (MAC, India). Composition of H_2 in evolved gas was analyzed by injecting $100 \mu\text{L}$ of a gas sample from the headspace of PBR into a gas chromatograph as described earlier by Basak et al. [53]. Concentration of VFAs and residual substrate was quantified by performing Reverse Phase Agilent 1260 Infinity HPLC (RPHPLC). 10 mL of fermentation broth was taken from the PBR and was centrifuged at 10000 rpm for 20 min in a refrigerated centrifuge (Eppendorf 5810R, Germany) at room temperature. Supernatant obtained after centrifugation was analyzed using a C-18 column (Agilent Eclipse Plus, $4.6 \times 250 \text{ mm}$, organosilane ligands, pore size $5 \mu\text{m}$) and diode array detector ($\lambda = 210 \text{ nm}$, temperature = $25 \text{ }^\circ\text{C}$, Agilent 1260). Column temperature was set at $55 \text{ }^\circ\text{C}$, and 0.05 moles of H_2SO_4 (filtered and degassed) was used as a mobile phase with a flow rate of 0.4 mL min^{-1} . Light intensity was measured with the help of a luxmeter (Lutron, Taiwan). HPR which is equivalent to the amount of H_2 gas produced per liter of culture per hour ($\text{mL L}^{-1} \text{ h}^{-1}$) in each batch performed was calculated as shown in Eq. 3:

$$\text{Hydrogen production rate (mL L}^{-1}\text{h}^{-1}) = \frac{V_{\text{hydrogen}}}{V_{\text{BR}} * t} \quad (3)$$

Where V_{hydrogen} is the volume of H_2 produced in mL, V_{BR} is the working volume of the bioreactor (L), and t is the time of H_2 production (h).

3 Optimization design and statistical analysis

3.1 Plackett-Burman design

The purpose of using the Plackett-Burman statistical design was to identify the most important process parameters for PF which affect the HPR capability of PNS bacteria. A total of 7 parameters were selected including OA concentration (X_1), temperature (X_2), pH (X_3), agitation rate (X_4), inoculum age of culture (X_5), inoculum concentration (X_6), and light intensity (X_7) as shown in Table 2. Each of the process variables was assigned -1 for low level and $+1$ for high level, and a total of 12 fermentation experiments were used for screening purposes. Table 3 represents the fermentation experiment along with experimental values of HPR (response). The experiments were performed in triplicate, and an average of HPR after 96 h of fermentation was taken into consideration. The significance of the each parameter was determined at 95% confidence level ($P < 0.05$). On the basis of results of the Plackett-Burman design, the process variables for H_2 fermentation were further optimized by RSM.

Table 2 Plackett-Burman design and regression analysis for screening important fermentative parameter for H₂ fermentation

Source	Low level (-1)	High level (+1)	Sum of square	df	Mean square	F-value	P value (prob > F)
Model	–	–	332.587	7	47.512	11.59	0.016
X ₁ : OA concentration	10	14	113.283	1	113.283	27.63	0.006 ^a
X ₂ : temperature	25	37	1.740	1	1.740	0.42	0.023 ^a
X ₃ : pH	5.5	7.5	25.433	1	25.433	6.20	0.067
X ₄ : agitation rate	150	250	3.819	1	3.819	0.93	0.389
X ₅ : inoculum age	24	48	105.317	1	105.317	25.68	0.007
X ₆ : inoculum concentration	5	10	77.673	1	77.673	18.94	0.012
X ₇ : light intensity	8	12	5.320	1	5.320	1.30	0.031 ^a

$R^2 = 95.30\%$; R^2 (adjust) = 87.08%

^aSignificant at 5% significance level

3.2 BBD matrix

BBD of RSM was used to optimize the screened parameters as suggested by the Plackett-Burman design for improving HPR. Minitab software 16.0 was used for this purpose. Based on the results of the Plackett-Burman design, the optimum level of OA concentration, temperature, and light intensity for maximum response and their effects as a function of linear, cross products, and quadratic interaction on H₂ production were determined by applying the BBD matrix. The range of three process parameters, dependent variables, and their corresponding levels for developing the regression model are shown in Table 4. The produced H₂ gas in the headspace region of PBR was measured after every 4 h. The total duration of PF was 96 h for each batch of

H₂ fermentation. Thereafter, HPR (mL L⁻¹ h⁻¹) was computed from the experimental data. Thereafter, regression analysis of the experimental HPR values was performed as a function of second order polynomial equation as shown in Eq. 4:

$$y = a_0 + \sum_{i=1}^k a_i x_i + \sum_{i=1}^k \sum_{j=1}^k a_{ij} x_i x_j + \sum_{i=1}^k a_{ii} x_i^2 \quad (4)$$

Here, “Y” is the predicted response, x_i are the input variables, a_0 is a constant term, and a_i , a_{ij} , and a_{ii} are the i th linear coefficient, ij th cross product coefficient, and quadratic coefficient respectively.

The model coefficients (linear, quadratic, and cross product terms) in the above equation can be calculated from the experimental value of HPR. In the case of three independent process variables with HPR as a response, Eq. 4 can be rewritten as

Volumetric hydrogen production rate

$$= \beta_0 + \beta_1 X_1 + \beta_2 X_2 + \beta_3 X_3 + \beta_{11} X_1^2 + \beta_{22} X_2^2 + \beta_{33} X_3^2 + \beta_{12} X_1 X_2 + \beta_{13} X_1 X_3 + \beta_{23} X_2 X_3 \quad (5)$$

Coefficient β_0 in Eq. 8 is offset coefficient; β_1 to β_3 are linear coefficients; β_{11} , β_{22} , and β_{33} are quadratic coefficients; and β_{12} , β_{13} , and β_{23} are interaction coefficients.

Here “-1” denotes the variation below the level giving maximum H₂ yield; “0” signifies the level of variables giving maximum H₂ yield; “+1” signifies the variation above the level of variable producing maximum H₂ yield

Table 3 Experimental matrix of Plackett-Burman design for HPR

Run order	X ₁	X ₂	X ₃	X ₄	X ₅	X ₆	X ₇	HPR (mL L ⁻¹ h ⁻¹)
1	1	-1	1	-1	-1	-1	1	25.25
2	1	1	-1	1	-1	-1	-1	20.76
3	-1	1	1	-1	1	-1	-1	22.00
4	1	-1	1	1	-1	1	-1	12.24
5	1	1	-1	1	1	-1	1	25.20
6	1	1	1	-1	1	1	-1	16.10
7	-1	1	1	1	-1	1	1	23.16
8	-1	-1	1	1	1	-1	1	18.22
9	-1	-1	-1	1	1	1	-1	16.00
10	1	-1	-1	-1	1	1	1	10.50
11	-1	1	-1	-1	-1	1	1	20.90
12	-1	-1	-1	-1	-1	-1	-1	21.00

Table 4 Independent variables and its corresponding levels for optimization of photo-fermentative H₂ production

Independent variables	Parameters	Unit	Low levels	Center levels	High levels
X ₁	OA concentration	g L ⁻¹	10	12	14
X ₂	Temperature (°C)	°C	25	31	37
X ₃	Light intensity	Klux	8	10	12

4 Development of mathematical models of photo-fermentative H₂ production system

4.1 Biochemical kinetics study of cell growth during PF by *R. sphaeroides* O.U.001 cells

Theoretically, the cell growth rate is expressed as follows:

$$\frac{dX}{dt} = \mu X \tag{6}$$

Where, *X* denotes the cell dry weight concentration in g L⁻¹ and μ corresponds to the specific growth rate in h⁻¹ which depends upon the concentration of the limiting substrate along with other factors.

In the present work, we developed an equation on the basis of a logistic model (nonstructured models used extensively to study microbial growth kinetics in a complex fermentation process) for determining the cell growth characteristics of *R. sphaeroides* O.U.001 cells during PF.

During the exponential phase, Eq. 6 gives

$$\mu_e = \frac{\ln\left(\frac{X_2}{X_1}\right)}{(t_2 - t_1)} \tag{7}$$

Where μ_e represents specific growth rate in the exponential phase and *X*₁ and *X*₂ are the cell concentrations in g L⁻¹ at times *t*₁ and *t*₂, respectively.

The cell growth kinetics during the entire growth curve (lag, exponential, and stationary phases) of *R. sphaeroides* O.U.001 were calculated as per logistic equation [54]:

$$\mu = K_c \left(1 - \frac{X}{X_{max}}\right) \tag{8}$$

Here, μ denotes specific growth rate in h⁻¹, *k_c* is the apparent specific growth rate in h⁻¹, and *X_{max}* is the maximum cell dry mass concentration in g L⁻¹.

By inserting Eq. 8 into Eq. 6 followed by integration, the following equation was obtained:

$$X = \frac{X_0 \exp(K_c t)}{1 - (X_0 / X_{max})(1 - \exp(K_c t))} \tag{9}$$

4.2 Substrate consumption kinetics during H₂ production using Monod model

Substrate utilization during batch fermentation is determined as per Eq. 10:

$$\frac{dS}{dt} = -\frac{1}{Y_{x/s}} \mu_s X \tag{10}$$

Here, *dS/dT* is the rate of substrate utilization, *Y_{x/s}* is the yield coefficient, μ_s is the specific growth rate in h⁻¹, and *X* is the cell dry mass concentration in g L⁻¹.

Dependency of *R. sphaeroides* O.U.001 growth rate during PF on DFCWE concentration was determined using the Monod model [55] as per Eq. 11:

$$\frac{1}{\mu_s} = \frac{K_s}{\mu_{max}} \frac{1}{[S]} + \frac{1}{\mu_{max}} \tag{11}$$

Values of maximum specific growth rate (μ_{max} , h⁻¹) and dissociation constant (*K_s*, g L⁻¹) were calculated with the Lineweaver-Burk linearized equation.

4.3 Kinetics of product formation and its relation with biomass growth during PF by *R. sphaeroides* O.U.001

Cumulative biohydrogen produced during PF was determined by fitting the modified Gompertz equation as per experimental data (Eq. 12):

$$P_i = P_{max,i} \exp\left\{-\exp\left[\frac{R_{max,e}}{P_{max,i}}(\lambda - t) + 1\right]\right\} \tag{12}$$

Where *P_i* is the H₂ accumulated (mL) at time *t* (h), *P_{max,i}* is the maximum cumulative H₂ (mL), *R_{max}* is the maximum HPR (mL L⁻¹ h⁻¹), λ is the lag time (h), *t* is the incubation time (h), and *e* = 2.718. The values of these kinetic parameters were determined by nonlinear fitting of cumulative H₂ production data using Origin pro software (version 8.5).

Further, relation between biohydrogen production at optimized conditions and growth of H₂-producing bacterial cells was determined by using the Luedeking-Piret equation [56].

$$\frac{dP_i}{dt} = \alpha_i \frac{dX}{dt} + \beta_i X \tag{13}$$

Here, α_i and β_i denote growth-linked and nongrowth-linked constant in h^{-1} , P_i is the cumulative H_2 production in mL, X is the cell dry mass concentration (g L^{-1}), and t is the fermentation time (h).

On further rearranging Eq. 13:

$$\frac{1}{X} \frac{dP_i}{dt} = \alpha_i \frac{1}{X} \frac{dX}{dt} + \beta_i \quad (14)$$

Here, $1/X dX/dt$ is the specific growth rate (μ) and $1/X dP_i/dt$ denotes specific HPR (v). Value of α_i and β_i can be determined from the slope and intercept of $1/X dP_i/dt$ versus $1/X dX/dt$ (during the exponential phase), respectively.

5 Results

5.1 Screening of important operational parameters for photo-fermentative H_2 production by using Plackett-Burman design matrix

The data of HPR as per experimental matrix of Table 3 indicated that there was a notable variation in H_2 production ranging from $10.50 \text{ mL L}^{-1} \text{ h}^{-1}$ to $25.25 \text{ mL L}^{-1} \text{ h}^{-1}$. Therefore, we felt the need of optimizing fermentation parameters for enhancing H_2 productivity. The parameters with the

confidence level greater than 95% and less than 95% were considered to have positive and negative impacts on H_2 productivity, respectively. As a result, the effect of OA concentration (X_1), temperature (X_2), and X_7 (light intensity) displayed a positive impact on HPR, whereas pH (X_3), agitation rate (X_4), inoculum concentration (X_6), and inoculum age (X_5) displayed a negative impact on HPR, which were not further included in the optimization study by the BBD matrix.

5.2 Optimization of fermentation parameters using BBD model for photo-fermentative H_2 production by *R. sphaeroides* O.U.001 cells

A total of 15 experimental combinations with three central points were performed in triplicate. The fermentation experiment designs along with experimental and predicted values of HPR are shown in Table 5, and HPR ($\text{mL L}^{-1} \text{ h}^{-1}$) recorded at different combination of OA, temperature, and light intensity was the average of data having variation within the range of 5%. The relationship between three fermentation parameters of H_2 production (OA concentration, temperature, and light intensity) was determined by BBD of RSM. Equation 15 represents the quadratic regression analysis for HPR, on the basis of actual data in coded form by using the software Minitab 16.0:

Table 5 15 BBD experimental matrix with three replicates defining OA concentration (g L^{-1} , X_1), temperature ($^{\circ}\text{C}$, X_2), and light intensity (klx, X_3) as independent variables and their corresponding HPR

Run	OA concentration (X_1 , g L^{-1})		Temperature (X_2 , $^{\circ}\text{C}$)		Light intensity (X_3 , klx)		HPR ($\text{mL L}^{-1} \text{ h}^{-1}$)	
	Coded value	Actual value	Coded value	Actual value	Coded value	Actual value	Actual ^a	Predicted
1	-1	10	-1	25	0	10	21.34	20.75
2	+1	14	-1	25	0	10	26.70	28.44
3	-1	10	+1	37	0	10	19.32	17.50
4	+1	14	+1	37	0	10	17.67	18.18
5	-1	10	0	31	-1	8	25.90	27.66
6	+1	14	0	31	-1	8	27.50	26.93
7	-1	10	0	31	+1	12	20.43	20.92
8	+1	14	0	31	+1	12	31.88	30.04
9	0	12	-1	25	-1	8	33.56	32.27
10	0	12	+1	37	-1	8	29.70	29.64
11	0	12	-1	25	+1	12	34.60	34.58
12	0	12	+1	37	+1	12	22.50	23.71
13 ^b	0	12	0	31	0	10	41.10	41.61
14 ^b	0	12	0	31	0	10	41.94	41.61
15 ^b	0	12	0	31	0	10	41.92	41.61

^a Average value of three experimental run

^b Center points

$$\begin{aligned} \text{HPR} = & 41.6533 + 2.0950 X_1 - 3.3762 X_2 - 0.9062 X_3 - 12.0292 X_1^2 \\ & - 8.3667 X_2^2 - 3.1967 X_3^2 - 1.7525 X_1 X_2 + 2.4625 X_1 X_3 - 2.0600 X_2 X_3 \end{aligned} \tag{15}$$

Here, HPR was the predicted response, and X_1 , X_2 , and X_3 were coded variables for OA concentration, temperature, and light intensity. Similarly, Eq. 16 represents the quadratic regression analysis for HPR, on the basis of actual data in uncoded form by using Minitab 16.0 software:

$$\begin{aligned} \text{HPR} = & -718.961 + 71.5935 X_1 + 17.3157 X_2 + 13.4644 X_3 - 3.00729 X_1^2 \\ & - 0.232407 X_2^2 - 0.799167 X_3^2 - 0.146042 X_1 X_2 + 0.615625 X_1 X_3 - 0.171667 X_2 X_3 \end{aligned} \tag{16}$$

Here, HPR is the experimental response, and X_1 , X_2 , and X_3 were actual values of all the three process variables. Based on the experimental results, minimum and maximum HPR was found to be 17.67 mL L⁻¹ h⁻¹ and 41.94 mL L⁻¹ h⁻¹, respectively.

The importance of each model term in the quadratic response surface model for the photo-fermentative H₂ production system was explored using statistical analysis such as analysis of variance (ANOVA), and their significance was

examined by checking the P value as shown in Table 6. The R^2 value for BBD matrix was 98.16% which means that only 1.84% variation in the PF system could not be explained by the chosen model. R^2 measures the goodness of fit of the model, and its value of 1.0 indicates that the regression model accurately fits the experimental data [57], though the adjusted R^2 value is more accurate in order to observe the accuracy of regression model. A good consistency was noted between adjusted and predicted R^2 values (94.84% and 91.20%, respectively) which implies that the chosen BBD model fits well with the experimental values of photo-fermentative H₂ production (Table 4). High Fisher variance ratio (F -value) of the model (129.61) and P value less than 0.05 implied that the regression model was significant. Lack-of-fit value was observed to be 24.86 which implies that the model was significant, and there were 1.9% chances that model F -value could occur due to noise. CV is the ratio of standard deviation (SD) of estimated data to the mean value of observed response. CV values notify about relative variability corresponds to the mean value, and a model having a value of CV less than 10% is considered reliable [58]. CV of 5.21% indicates that the chosen model is accurate in terms of linear, square, and interactive effects of process variables. ANOVA results revealed that at the α -level of 0.05, the BBD model was strongly

Table 6 ANOVA of quadratic polynomial model for HPR (mL L⁻¹ h⁻¹) by *R. sphaeroides* O.U.001 in BBD matrix

Factors	df ¹	Sum of squares ²	Mean square ³	F -value ⁴	P value prob > F ⁵
Model	9	937.644	104.183	129.61	0.001
X_1 (OA concentration, g L ⁻¹)	1	35.112	35.112	9.98	0.025
X_2 (temp, °C)	1	91.193	91.193	25.92	0.004
X_3 (light intensity)	1	6.570	6.570	1.87	0.230
X_1^2	1	468.578	534.280	151.87	0.000
X_2^2	1	244.946	258.466	73.47	0.000
X_3^2	1	37.731	37.731	10.72	0.022
$X_1 X_2$	1	12.285	12.285	3.49	0.121
$X_1 X_3$	1	24.256	24.256	6.89	0.047
$X_2 X_3$	1	16.974	16.974	4.82	0.029
R^2	–	–	0.9816	–	–
Adj- R^2	–	–	0.9484	–	–
Pred R^2	–	–	0.9120	–	–
Residual error	5	17.591	3.518	–	–
Lack of fit	3	17.131	5.710	24.86	0.019
Pure error	2	0.459	0.230	–	–
Correlation total	14	955.235	–	–	–
CV	–	0.0521	–	–	–

¹ df degrees of freedom

² Adj SS sum of square

³ Adj MS mean square

⁴ F -value: Fisher-Snedecor distribution value

⁵ P value: prob > F

statistically significant as the P value was less than 0.05. In this study, the linear effects of OA concentration, temperature, and quadratic effect of the three model terms, i.e., [OA concentration]², [temperature]², and [light intensity]², were highly significant (P value < 0.05). It was found that the linear effect of light intensity and cross interactive effects of operational variables (OA concentration, temperature, and light intensity) on photo-fermentative HPR was antagonistic in nature based on their P values (P value > 0.05). On the other hand, interaction between OA concentration and light intensity was found to have a synergistic effect on HPR during PF (P value = 0.047). None of the insignificant model terms has been eliminated from the ANOVA table in this work. Subsequently, the maximum predicted value of HPR (41.65 mL L⁻¹ h⁻¹) was obtained by solving the

regression Eq. 19 at optimum conditions of X_1 , X_2 , and X_3 with 12 g L⁻¹, 31 °C, and 10 klx, respectively.

5.3 Combined effects of OA concentration, temperature, and light intensity on HPR

Study of the interactive effect of operational parameters, i.e., OA concentration, temperature, and light intensity, on HPR during photo-fermentative H₂ production was evaluated by visual inspection of three-dimensional response surface and two-dimensional contour plots generated by Minitab 16.0 on the basis of Eq. 20 as shown in Figs. 2, 3, and 4. The graphs were generated by changing two continuous variables within the experimental range at a time and keeping the third variable at a constant value. The elliptical and circular shape of contour

Fig. 2 The 3D response surface plot (a) and its 2-dimensional contour plot (b) for photo-fermentative HPR (mL L⁻¹ h⁻¹) by *R. sphaeroides* O.U.001 in 2-L cylindrical PBR: interactive effects of OA concentration (g L⁻¹) and temperature (°C)

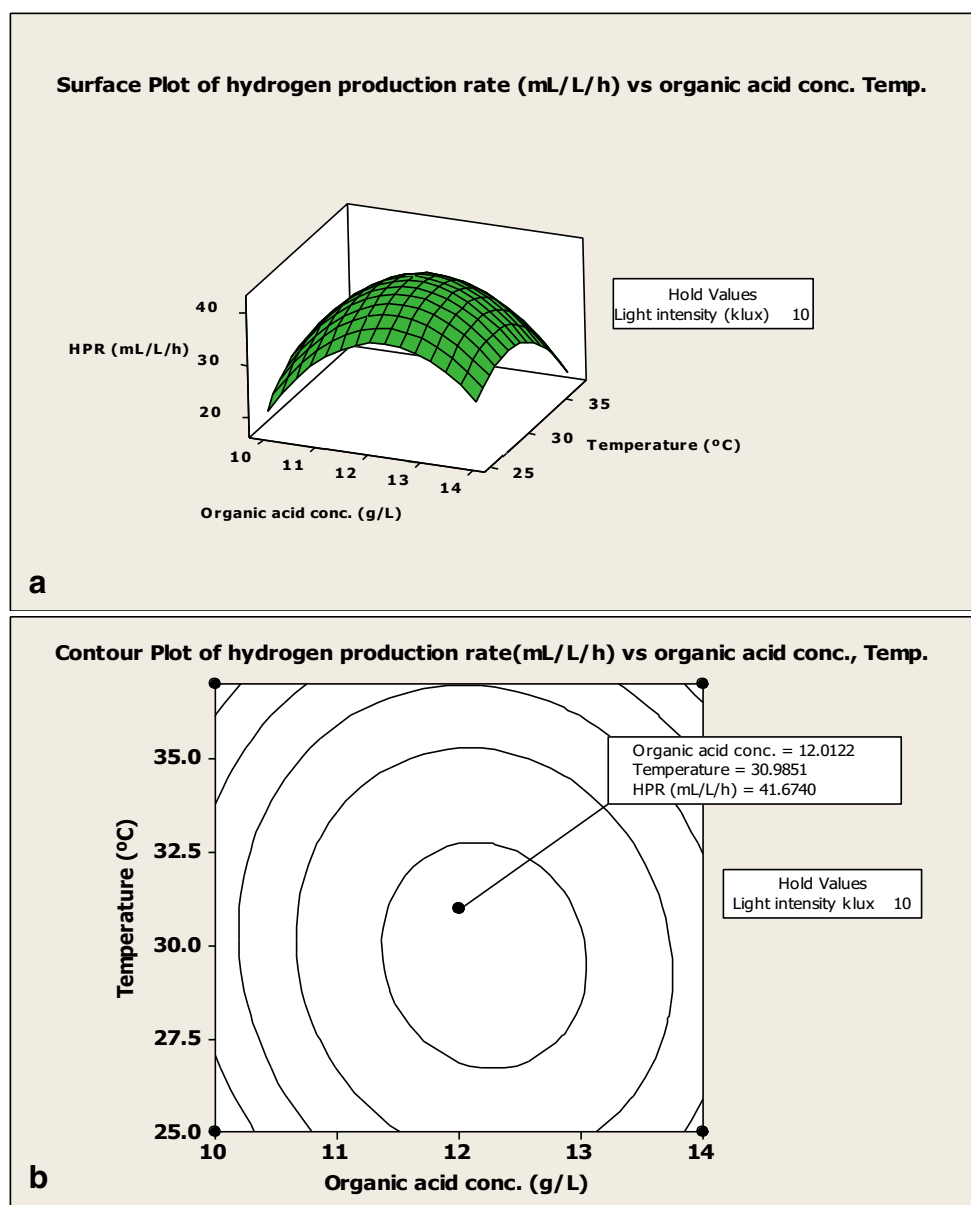
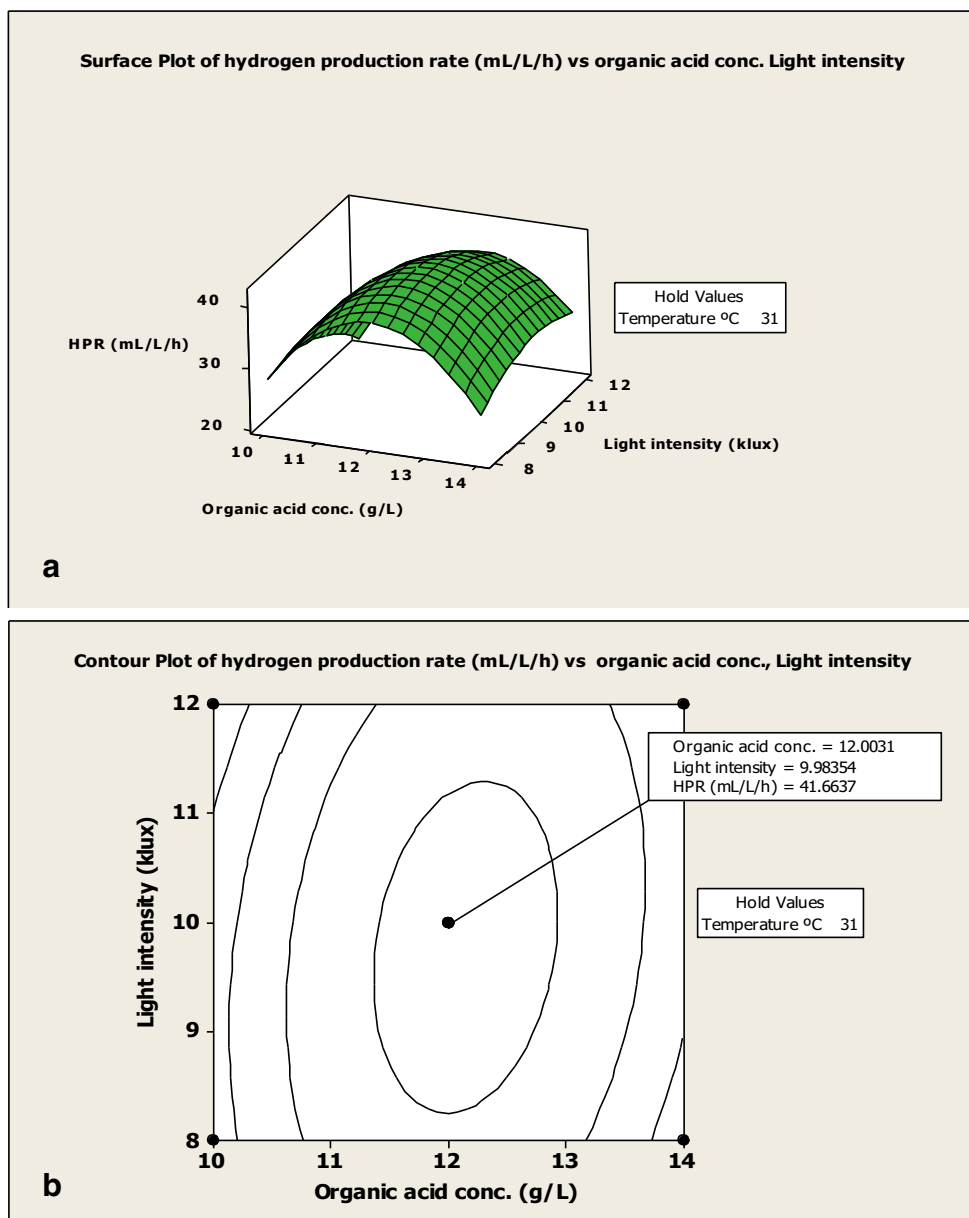


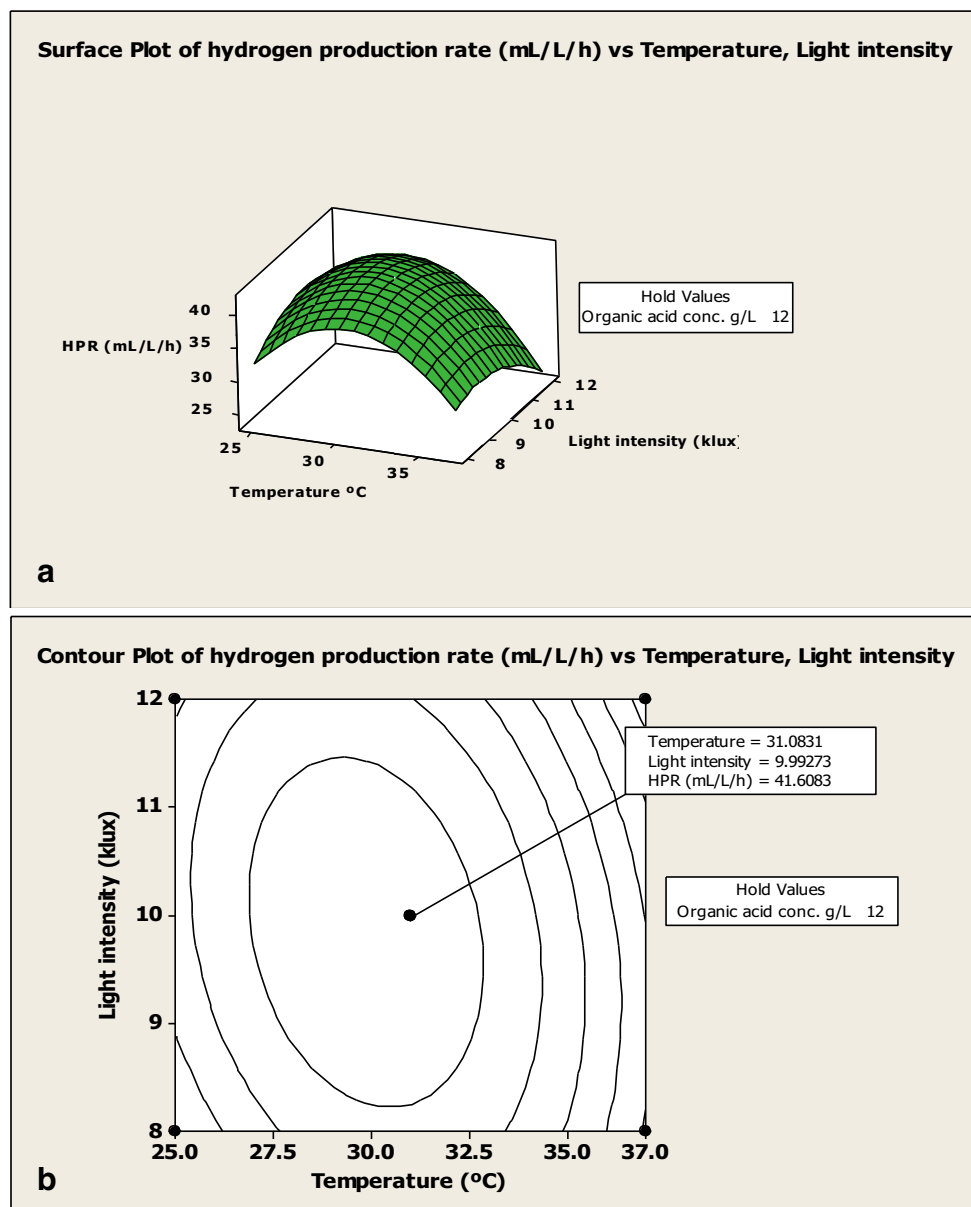
Fig. 3 The 3D response surface plot (a) and its 2-dimensional contour plot (b) for photo-fermentative HPR ($\text{mL L}^{-1} \text{h}^{-1}$) by *R. sphaeroides* O.U.001 in 2-L double-walled PBR: interactive effects of OA concentration (g L^{-1}) and light intensity (klx)



diagrams indicates significant and insignificant interactions between the process variables under observation [59]. Figure 2 shows the response surface and contour lines generated to evaluate the interactive effects of OA concentration and temperature by changing their values in a range of 10–14 g L^{-1} and 25–37 °C, respectively. Minitab holds the third variable (light intensity) at a constant level of 10 klx while calculating the fitted response value of HPR by *R. sphaeroides* cells. Statistically, the individual effects of OA concentration and temperature were found to be significant in improving HPR (P value = 0.025 for OA concentration and 0.004 for temperature). Presence of a clear peak in the response surface plot (Fig. 2a) suggests that the optimum conditions for OA concentration and temperature fell inside the design matrix.

With the change in the concentration of OA, the HPR changes which is almost similar to the surface with the change in temperature, thus demonstrating that both the parameters have a positive impact on the PF process for H_2 generation. When the value of OA concentration was kept fixed, HPR first increases up to a certain point, and then a decrease was observed on further increasing the temperature. Similarly, on keeping the temperature at a constant value, HPR first increases, and then decrease was observed on further increasing the OA concentration. Maximum predicted value for HPR was observed at the central peak point with OA concentration of 12 g L^{-1} and temperature of 31 °C. Rate of H_2 production was increased with increase in OA concentration from 10 to 12 g L^{-1} followed by a decline in production rate when the concentration of

Fig. 4 The 3D response surface plot and its 2-dimensional contour plot for photo-fermentative HPR ($\text{mL L}^{-1} \text{h}^{-1}$) by *R. sphaeroides* O.U.001 in 2-L cylindrical PBR: interactive effects of temperature and light intensity



the substrate was increased beyond 12 g L^{-1} . This is expected because a higher concentration of OA in the fermentation media resulted in substrate inhibition which leads to decrease in pH inside PBR. This inhibits the H_2 production efficiency of PNS bacteria. Further evidence related to dependency of H_2 production on substrate concentration is available in the literature. Sangyoka et al. [57] were of the view that going beyond the optimum concentration of the substrate in the PF system leads to the accumulation of partial pressure of H_2 gas in the headspace of PBR. As a result, the mechanism of bacterial cells is shifted towards the production of solvent instead of H_2 gas. It is an established fact that the rate of photo-fermentative H_2 production increases on increasing concentration of the substrate [60]. However, it has been noted that too much concentration of feedstock in the PBR could result

in higher concentration of bacterial cell thereby decreasing the biohydrogen yield. Previous research has studied the effect of substrate concentration on biohydrogen production by pure bacterial cells. Hitit et al. [61] reported the production of biohydrogen from potato juice by *Rhodospseudomonas* sp. and observed maximum H_2 production at a substrate concentration of 15 g L^{-1} . The PF process was inhibited on increasing the substrate load at a level higher than 15 g L^{-1} . This agrees with Sun et al. [62] who observed biohydrogen production with sucrose as the carbon source by co-culture of *Clostridium acidisoli* and *R. sphaeroides* during PF. Maximum hydrogen $5.08 \text{ mol mol}^{-1}$ hexose was obtained at an optimum substrate concentration of 11.43 g L^{-1} . Further, ability of bacterial cells to produce biohydrogen deteriorated when increasing the concentration of sucrose beyond 11.43 g

L^{-1} . The 2D contour plots of HPR versus OA concentration and temperature (Fig. 2b) was found to be elliptical in shape with maximum response occurring within the central contour region. This demonstrated the significant effect of their interaction on HPR. The same has been reported in literature where the elliptical nature of contour plots has resulted in significant interaction between the independent variables [37].

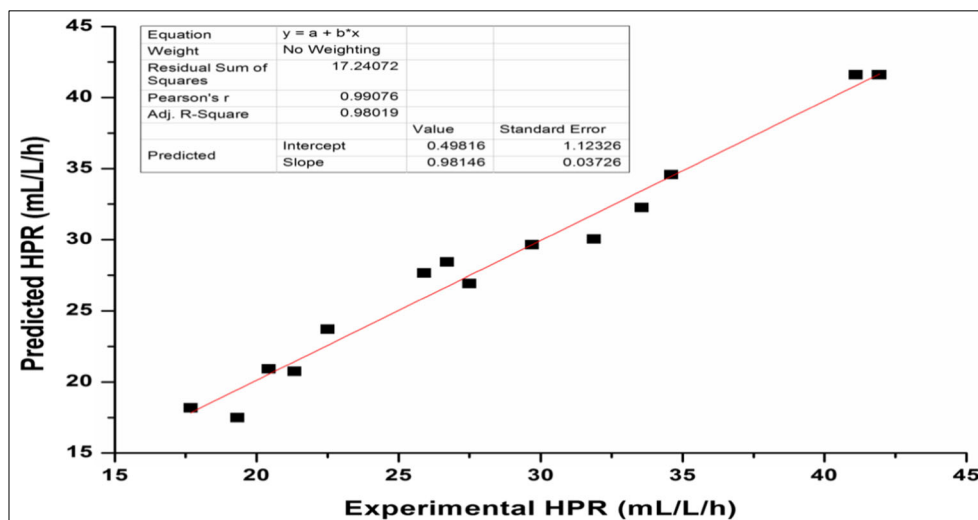
The graphical representation in Fig. 3 demonstrates the method to visualize the interactive effect of OA concentration and light intensity on H_2 production potential of *R. sphaeroides* O.U.001 to determine the optimum conditions. It can be observed from the response surface plot (Fig. 3a) that OA concentration and light intensity has greatly influenced the H_2 production. Temperature was kept constant at its central point, and the other two variables, i.e., OA concentration and light intensity, were varied within their experimental range of 10–14 $g L^{-1}$ and 8–12 klx, respectively. The highest HPR of 41.65 $mL L^{-1} h^{-1}$ was produced by PNS bacteria at optimal concentration of OA and light intensity (12 $g L^{-1}$ and 10 klx, respectively), keeping the temperature of the fermentation reaction constant at its uncoded value of 31 °C. Further increase in any of the two variables resulted in decline in HPR. This could be due to the fact that on further increasing the substrate concentration above 12 $g L^{-1}$, the viscosity of the fermentation media is increased which in turn may affect the mass transfer of the substrate to H_2 -producing bacterial cells. It is evident from the literature that PNS bacteria are sensitive to the operational parameters such as temperature, pH, presence of higher content of organic acid in fermentation medium, inhibition in the activity of nitrogenase enzyme due to high nitrogen load, and light intensity [13, 63]. Optimum range of light intensity is required by *R. sphaeroides* cells to achieve maximum HPR. From Fig. 3a, it can be analyzed that HPR is increased when illumination intensity is increased from 8 klx to 10 klx and then started to decrease on further increase of the values above the optimum point. The possible explanation for this behavior could be the availability of more ATP and ferredoxin at a higher light intensity (at 10 klx). This finding was found to be similar with a previous work [35]. In the current work, the maximum HPR was obtained at a light intensity of 10 klx beyond which the decline in production rate was noted. The light intensity was found to be in agreement with the optimal range of light intensity in previous reported works [23, 64]. Decrease in HPR on increasing the light intensity above 10 klx happened because at the light intensity above the optimum value, the bacterial cells experienced a cell shading effect and their photosynthetic apparatus is damaged due to which the overall light conversion efficiency is lowered thereby affecting the H_2 productivity. PNS bacteria have antenna molecules, i.e., up to 100 bacteriochlorophyll in each reaction center which helps them to survive during low availability of light [65]. But when the light intensity is abundant, there are chances that these antenna molecules may capture more photons than the capacity of photosynthetic machinery. As a

result, the antenna molecules are compelled to lose the H^+ ions in the form of heat/fluorescence due to which the cells which are present in the deep region inside the PBR encountered cell shading effect and their light conversion efficiency is hampered [66]. Therefore, during PF, illumination intensity of PBR is of great importance, and it must be controlled at an optimum level so that the metabolic pathway of PNS bacterial cells remains intact towards the production of H_2 gas. The 2D contour plot of interactive effects between OA concentration and light intensity on HPR by *R. sphaeroides* O.U.001 (Fig. 3b) was elliptical in shape indicating their synergistic effect on HPR. This was further confirmed by ANOVA results in Table 5 in which the *P* value for X_1X_3 was 0.047 (*P* value > 0.05). Castillo-Moreno et al. [23] reported 30.1 $mL L^{-1} h^{-1}$ of HPR using *Rhodobacter capsulatus* and a mixture of lactose and lactate as the substrate. The optimum concentrations of lactose and lactate were 19.17 and 2.61 $g L^{-1}$, respectively. These values were lower than the production rates obtained in the current study. Al-Mohammedawi et al. [35] observed higher HPR of 41.74 $mL L^{-1} h^{-1}$ using malic acid as a substrate by *R. sphaeroides* DSM 158 cells which was slightly lower than the values obtained in the current work.

The combined effect of temperature and light intensity on photo-fermentative H_2 production is shown in Fig. 4. It is evident that at a fixed OA concentration of 12 $g L^{-1}$, optimized temperature of 31 °C, and light intensity of 10 klx, maximum HPR achieved was 41.65 $mL L^{-1} h^{-1}$ (Fig. 4a). The optimum value of temperature in the current work falls in the reported range of temperature as mentioned in other studies [67, 68]. Temperature has an important role to enhance the fermentative H_2 yield during PF. It was seen that increase beyond the optimum value of fermentation temperature and light intensity produced a negative effect on the production rate of H_2 . Also, any increase above the optimum value adversely affects the metabolism of PNS bacteria due to heat stress effect and inactivation of cellular proteins such as proteases and chaperones, which in turn force the bacterial cell to revive its metabolic activities rather than produce biohydrogen [69]. On the other hand, when decreasing the temperature below the optimum level, there occurs a loss of cell fluids which in turn damages the viability of bacterial cells and H_2 productivity is negatively affected [70]. This is supported by previous research in which increasing the temperature above its optimum level during PF degenerates the nitrogenase enzyme activity which is a primary enzyme responsible for producing biohydrogen present in PNS bacteria and lowers the H_2 yield [26]. In the present work, significant interaction was observed between temperature and light intensity according to the shape of contour plots (Fig. 4b) and *P* value for X_2X_3 (0.029 determined by ANOVA).

Occurrence of a significant peak in the above-mentioned 3D response plots (Figs. 3, 4, and 5) and presence of clear maxima in their corresponding contour plots lead us to the

Fig. 5 Correlation between experimental and predicted HPR by *R. sphaeroides* cells in a 2-L PBR at optimal conditions



conclusion that the maximum value of predicted HPR could be identified within the design range.

5.4 Regression model analysis: correlation plot, the Anderson-Darling test, and residual plots for HPR

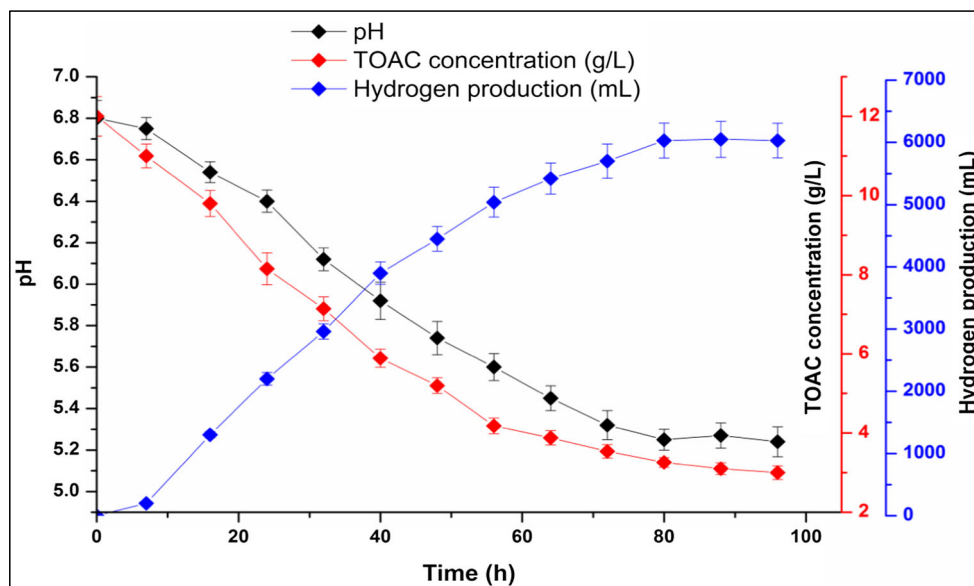
Predicted values of HPR at different experimental combinations in the cylindrical PBR were calculated by solving the regression Eq. 19. The correlation between experimental and predicted response at optimized conditions of OA concentration, temperature, and light intensity was found to be in good agreement (R^2 value 0.98) as shown in Fig. 5. The calculated value of R^2 indicates that the regression model is able to explain 98% of the variability in the response. The residuals (difference between predicted value and experimental value) help in knowing the important characteristics of the quadratic regression model. In this context, two residual plots, i.e., Anderson-Darling (AD) statistic normal probability plot and plot of residuals, versus the observed predicted value were used to confirm the fitting of the BBD model. The logic behind conducting the AD test was to confirm the normal distribution of residual error (predicted HPR minus experimental HPR). The associated P value of AD statistics was 0.435 and is proven to be significant (greater than α -level of 0.05) in determining normal distribution of the residual error as a function of OA concentration, temperature, and light intensity over the factorial space under consideration (Fig. 1 in supplementary materials). This confirms the suitability of the chosen BBD model for optimization purpose in the current work. Generally, residual plots are employed to determine the goodness of fit in the regression model and ANOVA. The plot between residual and fitted values helps in verifying the assumption that variance of the residuals at all the data points remains constant. The plot between residuals and predicted HPR (as shown in Fig. 2 in supplementary materials) revealed that the data points in the residual plot do not follow

any regular trend and are found to be randomly scattered. Variance in the residual plot is found to be constant for all values of predicted HPR. This indicates the better suitability of the chosen model in determining maximum predicted value of HPR at optimized values of independent variables.

5.5 Validation of experimental conditions for the BBD model

In the current study, we aimed to obtain the optimum conditions of three independent parameters for maximum HPR in the cylindrical PBR. The optimum conditions for better production rate suggested by the regression model were as follows: OA concentration 12 g L^{-1} , temperature $31 \text{ }^\circ\text{C}$, and light intensity 10 klx . At these optimal values, predicted HPR of $41.65 \text{ mL L}^{-1} \text{ h}^{-1}$ was obtained (by solving the regression equation). To confirm the reliability of the chosen BBD model, confirmatory experiment in triplicate was done at the optimum values of variables. At these conditions, cumulative H_2 production of 6050 mL L^{-1} of media was produced with experimental HPR of $41.96 \text{ mL L}^{-1} \text{ h}^{-1}$, which was found to be in reasonable agreement with predicted value of $41.65 \text{ mL L}^{-1} \text{ h}^{-1}$. Profile of cumulative H_2 produced, change in pH, and substrate utilization are shown in Fig. 6. Production of H_2 in PBR started after 7 h of inoculation which can be considered as the lag phase of bacterial cell towards fermentation media. Growth of PNS cell followed the expected pattern of exponential and stationary phases. The notable decrease in initial pH (from 6.75 at 7 h to 6.54 h at 16 h) was also observed after the lag phase which continued up to 80 h and thereafter becomes almost constant. The same pattern was observed in the case of photo-fermentative H_2 production. After 7 h, the cells in the logarithmic period utilized OA for producing H_2 , and significant increase in H_2 production, i.e., from 200 mL at 7 h to 6050 mL L^{-1} at 88 h, was observed up to the time the cells enter into the stationary phase. Consumption of OA by PNS

Fig. 6 Validation of regression model for H₂ production at optimum conditions showing cumulative H₂ produced, pH profile, and substrate utilization by *R. sphaeroides* O.U.001 spent medium



bacteria from the fermentation media under optimal conditions was 32%, 57%, 70%, and 75% at the corresponding time interval of 24 h, 48 h, 72 h, and 96 h, respectively, with 3 g L⁻¹ of residual concentration of OA (75% utilization yield). Hence, the utilization of DFCWE for subsequent PF by PNS bacterial cells in the batch mode and statistical optimization of technological variables for H₂ production by RSM model were practical and valid. Further, the optimization result confirmed the validity of the second-order polynomial regression equation used in the current work for enhancing photofermentative HPR.

6 Fitting of mathematical models parameters with experimental data of batch H₂ fermentation under optimized conditions

6.1 Kinetics of *R. sphaeroides* O.U.001 cells during PF

Use of logistic Eq. 9 shows that the *R. sphaeroides* cell inside PBR follows a typical growth pattern under optimum conditions of fermentation parameters. Values of maximum cell biomass concentration (X_{max}) and apparent specific growth rate (K_c) were modelled by fitting experimental cell mass concentration to the logistic equation, giving their respective values as 18.06 g L⁻¹ and 0.04 h⁻¹. Values of X_{max} and K_c were found to be quite similar to that of experimental values. Biomass concentration (g L⁻¹) simulated by the logistic model gave an adjacent R^2 value of 99.3%, illustrating adequate agreement of the logistic model in terms of growth profile of H₂-producing cells as shown in Fig. 7a.

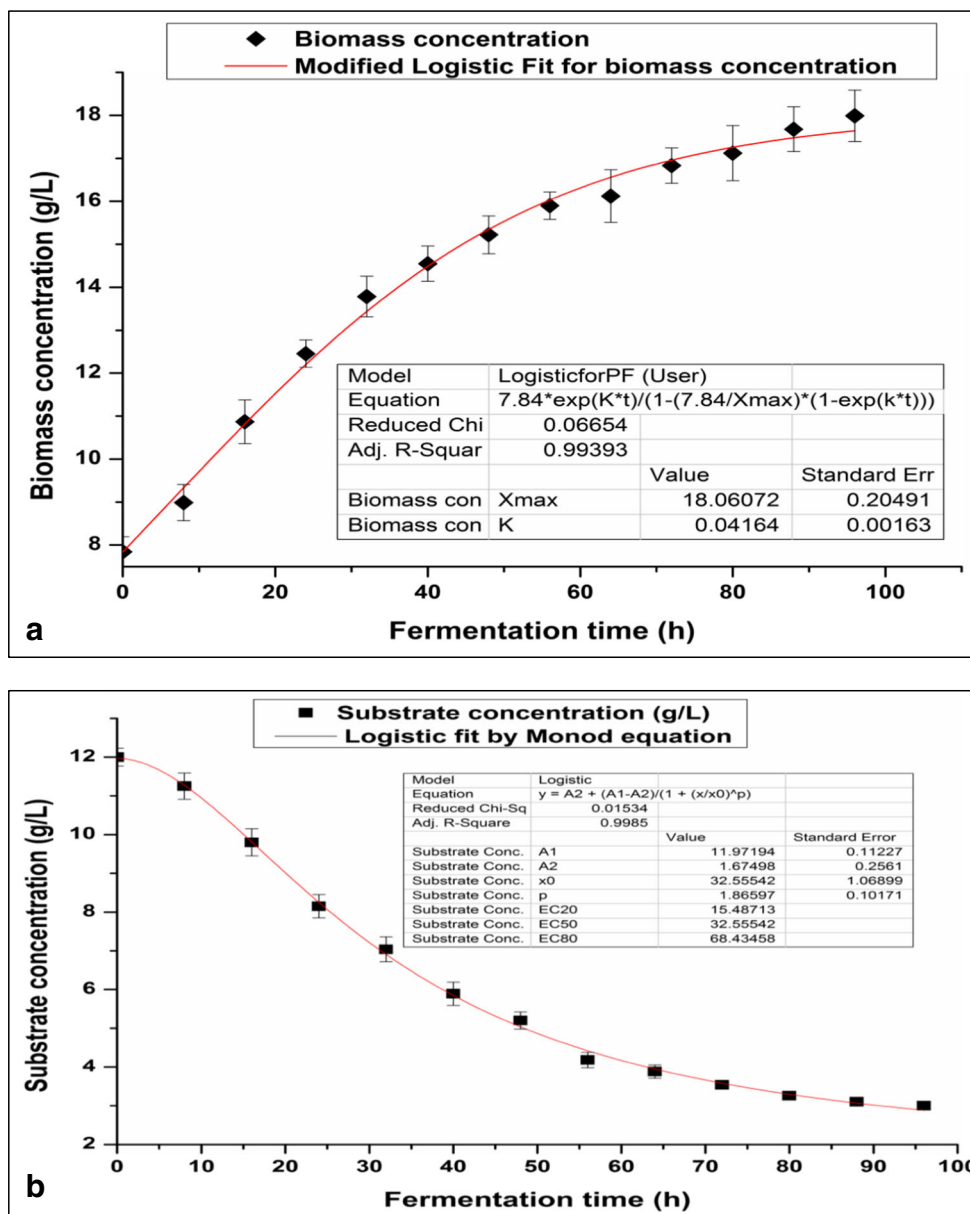
6.2 Mathematical modelling of substrate consumption in PF by *R. sphaeroides* O.U.001 using Monod model (DFCWE as substrate)

The Monod model was employed for determining the consumption of DFCWE during PF by *R. sphaeroides* O.U.001. Estimation of the specific growth rate (μ_{max}) and saturation constant (K_s) was done by using the Lineweaver-Burk plot, and their values were found to be 0.92 h⁻¹ and 12.45 g L⁻¹, respectively. Value of μ_{max} is dependent upon the fermentation temperature and pH of fermentation media [71]. Although temperature was kept constant at 31 °C, pH was decreasing with time which lowered the μ_m . Experimental values of DFCWE utilization were fitted into Eq. 14 which gave an adj. R^2 value of 99.8%, thus confirming a satisfactory correlation between the model and experimental values as shown in Fig. 7b. Further, in the current work, concentration of the initial substrate during batch PF was less than the value of K_s , which signifies the positive growth of H₂-producing microbes under optimum conditions of process variables.

6.3 Kinetics of H₂ formation during PF by *R. sphaeroides* O.U.001 (DFCWE as substrate) using modified Gompertz equation

Cumulative H₂ obtained during PF were simulated by nonlinear fitting into the modified Gompertz equation, and values of kinetic parameters (H_{max} , R_{max} , and λ) were calculated by best fitting the experimental data of HPR into Eq. 12. Higher R^2 value of 99.76% as shown in Fig. 8a indicated strong correlation between experimental

Fig. 7 a *R. sphaeroides* cells growth fitting to logistic model. **b** Fitting of experimental data to Monod model for DFCWE concentration during PF by *R. sphaeroides* O.U.001



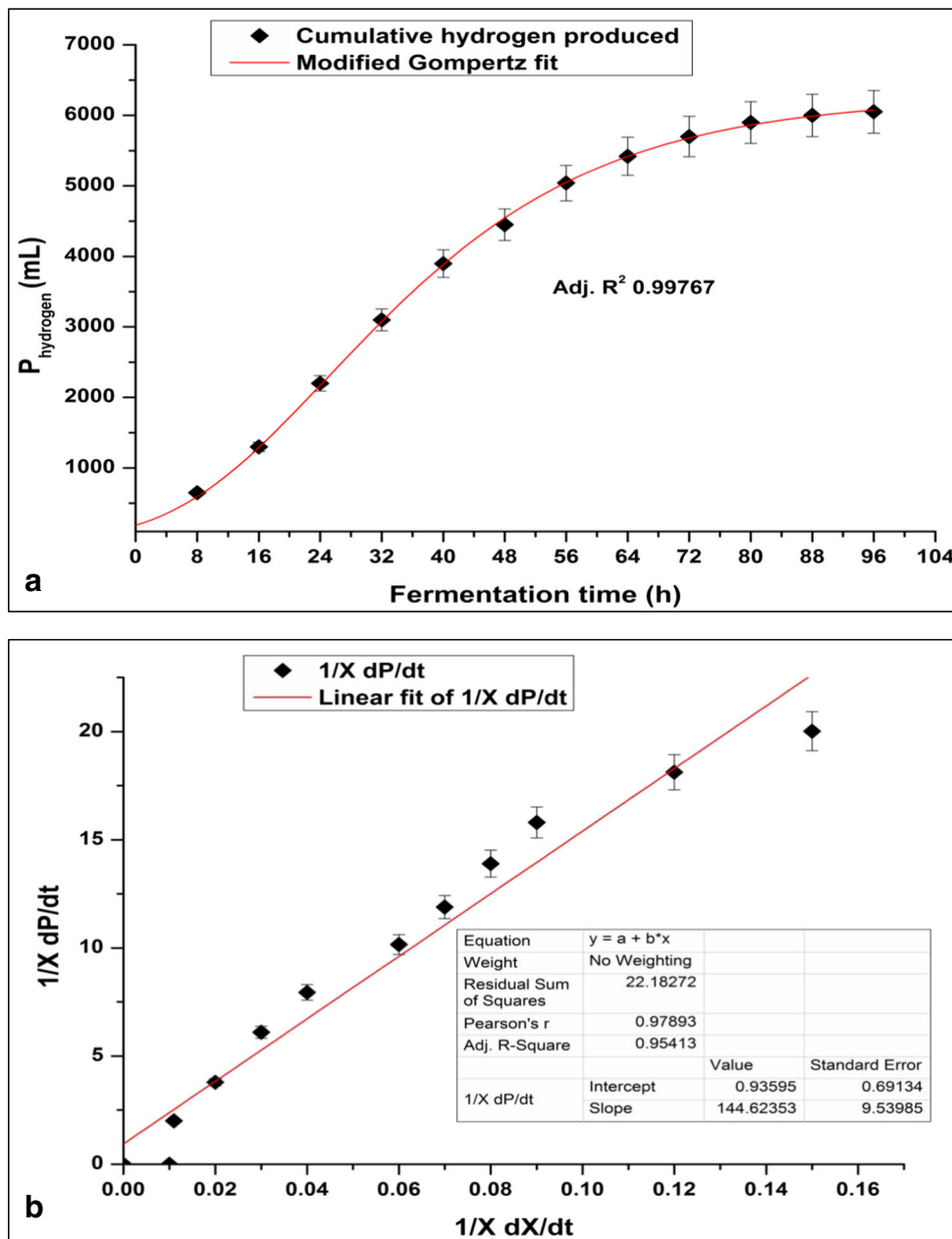
values and the modified Gompertz equation to interpret H_2 production kinetics in the current work. However, some difference in the values of cumulative H_2 production and lag phase was observed. The experimental value of cumulative H_2 production was found to be 6050 mL under optimum operational conditions in the presence of 12 g L^{-1} of DFCWE with a lag phase of 8.5 h, whereas the predicted value of cumulative H_2 production by modified Gompertz equation was 6080.9 mL with a lag phase of 6.55 h. Further, the predicted value of HPR during the total batch time of 96 h was $36.68 \text{ mL L}^{-1} \text{ h}^{-1}$ as compared to the experimental HPR of $41.94 \text{ mL L}^{-1} \text{ h}^{-1}$. The variation in predicted and measured values of kinetic parameters of the modified Gompertz equation was due to

the viability of H_2 -producing microbes. However, there exists variation in the value of kinetic parameters due to different experimental conditions such as feedstock and time taken by bacterial cells to adapt to environment before producing H_2 .

6.4 Kinetic relationship between biomass growth and H_2 production during batch H_2 fermentation by the Luedeking-Piret model

Experimental cumulative H_2 obtained during batch fermentation were fitted into Eq. 14. The correlation coefficient (adj. R^2) was 95.41% indicating proper fitting of the experimental data with the Luedeking-Piret model. Values

Fig. 8 **a** Nonlinear fitting of modified Gompertz equation with experimental HPR for *R. sphaeroides* O.U.001. **b** Luedeking-Piret plot explaining relationship between biomass and HPR



of α (constant for growth-linked product) and β (constant for nongrowth-linked product formation) were found to be 144.62 mL L^{-1} and 0.94 mL h^{-1} , respectively, which show that *R. sphaeroides* O.U.001 exhibited mixed growth-associated product formation as shown in Fig. 8b. Moreover, the magnitude of α could be used to determine the H_2 productivity in batch PF, and it further explains the dependency level of H_2 production on the specific growth rate. Table 7 shows the comparison of different kinetic parameters of the logistic model, Monod model, modified Gompertz equation, and Luedeking-Piret model obtained in the current work with those reported in the literature.

7 Discussion

It is evident from the literature that quite a number of significant studies related to photo-fermentative H_2 production have been carried in the past years using different bacterial strains (pure culture or microbial consortia) and feedstock (ranging from simple sugars to industrial effluents) under different sets of operation parameters. A comparative study of optimum conditions of process variables (with or without statistical optimization tool) obtained in the present work with the literature is summarized in Table 8. The table shows that fermentation was performed at different sets of operating conditions such as inoculum concentration, temperature, pH, light intensity, and

Table 7 Comparison of kinetic parameters obtained in current work with those available in literature

Substrate and concentration	Inoculum	WV _{bioreactor} (L)	Logistic model parameters			Monod model parameters			Modified Gompertz equation parameters			Luedeking-Piret model parameters			Ref
			X_{\max}	K_c	R^2	K_s	μ_{\max}	H_{\max}	R_{\max}	λ	R^2	Nature of product	α	β	
Malic acid, 1.01 g L ⁻¹	<i>R. sphaerooides</i> O.U.001	0.4	0.98 g L ⁻¹	0.06 h ⁻¹	0.98	Not performed	Not performed	Not performed	Not performed	Not performed	Not performed	Not performed	Not performed	[51]	
Effluent of dark fermented glucose, 10 g L ⁻¹	<i>R. sphaerooides</i> O.U. 001	0.6	0.44 g L ⁻¹	0.09 h ⁻¹	0.99	5.51 g L ⁻¹	0.4 h ⁻¹	615.65 mL	16.15 mL h ⁻¹	14.32 h	0.97	Not performed	Not performed	[54]	
Effluent of dark fermentative sucrose	<i>Rhodospseudomonas palustris</i> WP3-5	0.26	Not performed	Not performed	Not performed	Not performed	Not performed	169.3 mL	2.1 mL L ⁻¹ h ⁻¹	3.40 h	0.97	Not performed	Not performed	[72]	
Dairy wastewater	<i>R. sphaerooides</i> O.U.001	0.0125	Not performed	Not performed	Not performed	Not performed	Not performed	2520 mL	57 mL L ⁻¹ h ⁻¹	18 h	0.98	Not performed	Not performed	[44]	
Lactate and succinate	<i>R. sphaerooides</i> RV	0.32	Not performed	Not performed	Not performed	Not performed	Not performed	56.5 mL	1.98 mL L ⁻¹	28.3 h	0.97	Not performed	Not performed	[73]	
Glucose, 16 g L ⁻¹	Mixed consortia	0.7	30.74 g L ⁻¹	0.061 h ⁻¹	0.94	0.11 g L ⁻¹	0.17 h ⁻¹	Not performed	Not performed	Growth linked	0.99	11.05	0.002	[74]	
Dairy wastewater, 15.3 g COD L ⁻¹	Anaerobic sludge	1	7.26 g VSS L ⁻¹	15.89 g COD ⁻¹	0.96	15.89 g COD L ⁻¹	0.64 h ⁻¹	2283.57 mL	116.32 mL L ⁻¹ h ⁻¹	4.08 h	0.99	Not performed	Not performed	[75]	
Malate	<i>R. sphaerooides</i> K KU-PSS	0.07	Not performed	Not performed	Not performed	Not performed	Not performed	1046 mL L ⁻¹	4.39 mL L ⁻¹ h ⁻¹	50.46 h	0.99	Not performed	Not performed	[25]	
Malic acid, 2.01 g L ⁻¹	<i>R. sphaerooides</i> O.U. 001	1	1.35 g L ⁻¹	0.052 h ⁻¹	0.98	NR	NR	700 mL L ⁻¹	7 mL L ⁻¹ h ⁻¹	14 h	0.99	Mixed growth	Mixed growth	[53]	
Potato waste	<i>Rhodobacter</i> sp., <i>Rhodospirillum</i> sp., <i>Rhodospseudomonas</i> sp., <i>Rhodospirillum</i> sp., <i>Rhodospseudomonas</i> sp.	0.15	Not performed	Not performed	Not performed	Not performed	Not performed	659 mL	9.7 mL h ⁻¹	0.04 h	0.99	Not performed	Not performed	[76]	
Effluent of dark fermented com straw	<i>Rhodobacter</i> sp., <i>Rhodospirillum</i> sp., <i>Rhodospseudomonas</i> sp., <i>Rhodospirillum</i> sp., <i>Rhodospseudomonas</i> sp.	0.18	Not performed	Not performed	Not performed	Not performed	Not performed	365.6	28.06 mL h ⁻¹	2.45 h	0.98	Not performed	Not performed	[2]	
Effluent of dark fermented CW	<i>R. sphaerooides</i> O.U.001	1.5 L	18.06 g L ⁻¹	0.04 h ⁻¹	0.99	12.45 g L ⁻¹	0.92 h ⁻¹	6080.9 mL	36.68 mL L ⁻¹ h ⁻¹	6.55 h	0.99	Mixed growth	Mixed growth	144.62 0.94 0.95 This study	

Table 8 Comparison of optimization results obtained in this study with published data related to batch PF

Inoculum used	Carbon source and concentration	WV (L)	operating conditions		Regression model used (yes/no)	Parameters studied and its optimum value	Response (HC/HPR)	Ref	
			T (°C)	pH					Light intensity
<i>R. capsulata</i>	Acetate, propionate butyrate; OA conc. (3 g L ⁻¹)	NR	32	7.31	4 klx	Yes, CCD	Glutamate conc.: 1.03 g L ⁻¹ pH: 7.31	19.25	[77]
<i>R. sphaeroides</i> O.U. 001	Malate (2.01 g L ⁻¹)	0.55	30–33	6.6–6.8	270 W m ⁻² (tungsten)	No	Substrate conc.: 1.832 g L ⁻¹	33	[78]
<i>Rhodospseudomonas palustris</i> WP3-5	Butyric acid (1–2 g L ⁻¹)	0.1	32	7.1	10 klx (tungsten)	Yes, CCD	Glutamic acid: 607 mg L ⁻¹ FeCl ₃ : 54 mg L ⁻¹	24.7	[64]
<i>R. sphaeroides</i> O.U.001	Malate (2.01 g L ⁻¹)	1	32	6.8	15 W m ⁻² (tungsten)	No	–	6.5	[79]
<i>R. sphaeroides</i> O.U. 001	Malate (2.01 g L ⁻¹)	0.055	30–33	6.7	150–200 W m ⁻² (tungsten)	No	–	24	[16]
<i>Rhodospseudomonas palustris</i> NiFA*	Vegetable waste (acetic acid, lactic acid and NH ₄ ⁺); OA conc. (10 g L ⁻¹)	NR	30	6.8	35 mmol m ² s ⁻¹ (tungsten)	No	–	9.6	[80]
<i>R. sphaeroides</i> O.U. 001	Malate (2.01 g L ⁻¹)	0.17	32	6.5	102 W m ⁻² (halogen)	No	–	41.9	[81]
<i>R. capsulatus</i> DSM 1710	Acetic acid (2.4 g L ⁻¹)	0.05	27.5	6.4	287 W m ⁻² (halogen)	Yes, FFD	Same as operating conditions	12.6	[34]
Mixed consortium	Acetate, propionate, and butyrate; OA conc. (3.51 g L ⁻¹)	NR	30–35 °C	6.8	5 klx (tungsten)	Yes, CCD	Acetate: 1.18 g L ⁻¹ Propionate: 0.74 g L ⁻¹ Butyrate: 1.59 g L ⁻¹	6.1	[82]
<i>R. sphaeroides</i> O.U.001	Malate (2.68 g L ⁻¹)	1	33 °C	6.8	15 W m ⁻² (tungsten)	Yes, FFD	Substrate conc.: 2.68 g L ⁻¹ Glutamate conc.: 0.59 g L ⁻¹ FeCl ₃ conc.: 0.05 g L ⁻¹	7	[53]
<i>R. palustris</i> CGA676	Wheat bran (WB) effluent (7.46 g L ⁻¹ VFAs) and corn (8.67 g L ⁻¹ VFAs)	0.1	30 °C	6.8	200 μmol m ⁻² s ⁻¹ (tungsten)	No	–	HPR _{WB} : 11.60 HPR _{corn} : 3.82	[83]
<i>R. capsulatus</i> DSM 1710	Dark fermentative effluent (lactose, lactic, butyric, acetic, and propionic acid); OA conc. (31.78 g L ⁻¹)	0.7	35 °C	6.8	338 W m ⁻² (mercury lamp)	No	–	208.40 mmol L ⁻¹ d ⁻¹	[84]
<i>R. sphaeroides</i> DSM 158	Malate (2.68 g L ⁻¹)	0.12	–	7.4	126 W m ⁻² (halogen)	Yes, BBD	Same as operating conditions	41.74	[35]
<i>R. capsulatus</i> B10	Lactose (21.2 g L ⁻¹) and lactate (1.62 g L ⁻¹)	0.125	30 °C	7.03	23.35 klx (tungsten)	Yes, CCD	pH: 7.03 Lactose conc.: 21.22 g L ⁻¹ Lactate conc.: 1.62 g L ⁻¹ Glutamate conc.: 6.62 g L ⁻¹ mM Light intensity: 23.35 klx	41.5	[23]
<i>R. capsulatus</i> IR3	Lactose (19.17 g L ⁻¹) and lactate (2.61 g L ⁻¹)	0.125	30 °C	6.94	26.97 klx (tungsten)	Yes, CCD	pH: 6.94 Lactose conc.: 19.17 g L ⁻¹ Lactate conc.: 2.61 g L ⁻¹ Glutamate conc.: 7.36 g L ⁻¹ Li: 26.97 klx	30.1	[23]
<i>R. sphaeroides</i> O.U.001	Effluent of dark fermented CW; OA conc. (12 g L ⁻¹)	1.5	31 °C	6.8	8–10 klx (CFL + LED)	Yes, BBD	Substrate conc.: 12 g L ⁻¹ Temperature: 31 °C Light intensity: 10 klx	41.94	This study

agitation rate which was responsible of the difference in optimum values of process parameters and HPR. The rate of biohydrogen production varies from $6.1 \text{ mL L}^{-1} \text{ h}^{-1}$ which was obtained using a mixture of acetate, propionate, and butyrate as carbon source at $30\text{--}35 \text{ }^\circ\text{C}$ of temperature, initial pH of 6.8, and light intensity of 5 klx [82] to $41.9 \text{ mL L}^{-1} \text{ h}^{-1}$ acquired using pure malate as the carbon source by *R. sphaeroides* O.U.001 cells at $32 \text{ }^\circ\text{C}$ of temperature and initial pH of 6.5 under the illumination of 102 W m^{-2} of light intensity [81]. Also, the working volume of PBRs in the studies mentioned in the table is in the range of 0.05–1 L. Comparative analysis shows that malic acid has been a preferable choice for producing biohydrogen during PF. Also, pure lactose and lactate [23] have produced more biohydrogen than butyric [64] and acetic acid alone [34]. The photo-fermentative HPR obtained in the current study using DFCWE was found to be impressive as compared to other reported research. The HPR achieved by *R. sphaeroides* cells at optimal conditions of OA concentration, temperature, and light intensity in the current work was quite high as compared to those obtained by Basak et al. [33], Basak et al. [53], Al-Mohammedawi et al. [35], Zagrodnik et al. [81], Uyar et al. [78], and Uyar et al. [16] while working with the same bacterial strain having a working volume of PBR as 1 L, 1 L, 0.12 L, 0.17 L, 0.55 L, and 0.055 L respectively. Basak et al. [53] reported HPR of $7.0 \text{ mL L}^{-1} \text{ h}^{-1}$ from malic acid substrate by *R. sphaeroides* O.U.001 cells at a substrate concentration, temperature, and light intensity of 2.68 g L^{-1} , $33 \text{ }^\circ\text{C}$, and 15 W m^{-2} , respectively. In another work done by Androga et al. [34], full factorial design matrix was used to optimize the process parameters, and maximum HPR of $13 \text{ mL L}^{-1} \text{ h}^{-1}$ was achieved by *R. capsulatus* DSM 1710 at acetic acid concentration, temperature, and light intensity of 2.40 g L^{-1} , $27.5 \text{ }^\circ\text{C}$, and 4.2 klx, respectively. Castillo-Moreno et al. [23] used a central composite design of RSM and reported HPR of $41.5 \text{ mL L}^{-1} \text{ h}^{-1}$ at a substrate concentration of 22.84 g L^{-1} , temperature of $30 \text{ }^\circ\text{C}$, and light intensity of 23.35 klx. Also, the experimental HPR in the present work was higher than those produced by other H_2 -producing bacterial cultures such as *R. capsulatus* [23, 34, 77, 84], *Rhodospseudomonas* sp. [39, 64, 80, 83], and mixed consortia [82] (Table 8). Nevertheless, the HPR was smaller than those by *R. sphaeroides* DSM 158 [85] and *R. sphaeroides* ZX5 [86]. For example, HPR of $102.33 \text{ mL L}^{-1} \text{ h}^{-1}$ was recorded by Li et al. at 4 g L^{-1} of malic acid, fermentation temperature of $30 \text{ }^\circ\text{C}$, and light intensity of 4–5 klx [86], whereas in the present study, HPR of $41.94 \text{ mL L}^{-1} \text{ h}^{-1}$ was obtained at 12 g L^{-1} , $31 \text{ }^\circ\text{C}$, and 10 klx of organic acid concentration, temperature, and light intensity, respectively. The usual justification for getting variations in the results from different studies is the composition and extent of utilization of different carbon and nitrogen sources and experimental conditions, specifically the source of light and its illumination intensity. Mishra et al. [37] and Al-

Mohammedawi et al. [35] also explained that the concentration of substrate, its composition (simple sugar or agricultural waste, etc.), and illumination intensity should be optimized carefully as a change in both of these parameters can affect the activity of nitrogenase enzyme present in PNS bacterial cells. With the same optimization tool, the cumulative amount of biohydrogen produced at optimum operative variables in the current work was 6050 mL L^{-1} which was higher than those reported by Dolly et al. [24], Al-Mohammedawi et al. [35], and Garimella et al. [67]. Hence, utilization of DFCWE as a raw material for producing biohydrogen by PNS bacteria in double-walled cylindrical PBR (with a working volume of 1.5 L) has certain reference value. Further use of the BBD matrix for designing the PF experiment was found to be useful for optimizing the three important process parameters.

8 Conclusion

In the current work, dark fermentative cheese whey effluent (DFCWE) was used as feedstock for photo-fermentative H_2 production using *R. sphaeroides* cells. The HPR was investigated at varying levels of OA concentration, temperature, and light intensity by response surface methodology. The maximum HPR of $41.94 \text{ mL L}^{-1} \text{ h}^{-1}$ was obtained under the optimized conditions: OA concentration 12 g L^{-1} , temperature $31 \text{ }^\circ\text{C}$, and light intensity 10 klx. The validation experiment for the obtained optimal conditions for H_2 production from DFCWE had adequate agreement with the predicted values $41.65 \text{ mL L}^{-1} \text{ h}^{-1}$. 3D response surface plots revealed that the optimal point for all the three variables fell inside the boundary range. Further, modelling of the photo-fermentative system revealed that the experimental data for the consumption of substrate and biomass concentration and for batch H_2 production analysis by PNS bacteria gave satisfactory simulated results. The Lineweaver-Burk plot for substrate utilization by PNS bacteria in PF gave the values of μ_{max} and K_s as 0.92 h^{-1} and 12.45 g L^{-1} , respectively, under uncontrolled pH of production media. Values of logistic constant, i.e., X_{max} and K_c , as a function of fermentation time, during the batch test, were 18.06 g L^{-1} and 0.04 h^{-1} , respectively. Also, nonlinear curve fitting of observed H_2 with modified Gompertz equation was in close agreement with the predicted values of cumulative H_2 produced ($P_{\text{max},i}$), maximum HPR (R_{max}), and lag time (λ) as 6080.9 mL , $36.68 \text{ mL L}^{-1} \text{ h}^{-1}$, and 6.55 h, respectively, at an optimized concentration of 12 g L^{-1} of OA. The experimental results may offer valuable knowledge for upscaling photo-fermentative H_2 production process and for designing efficient PBRs for better photo-fermentative H_2 productivity. Some of the future recommendations based on the current outcome are (i) immobilization of the *R. sphaeroides* bacterial cell using transparent matrix; (ii) building and selection of H_2 impermeable PBR by keeping in mind uniform distribution of

light at each corner of the PBR; (iii) implementation of genetic engineering in order to manipulate key enzymes (hydrogenase, nitrogenase) and upgrade light conversion efficiency of PNS bacteria; and (iv) enhancing photo-fermentative H₂ productivity by applying CFD simulation in order to predict flow pattern, distribution of light, and temperature of fermentation liquid inside the PBR.

Supplementary Information The online version contains supplementary material available at <https://doi.org/10.1007/s13399-021-01377-1>.

Acknowledgements The first author, Raman Rao, wishes to thank the Ministry of Human Resource & Development, under the aegis of the Government of India for providing the fellowship. The authors are indebted to the Dr. B R Ambedkar National Institute of Technology Jalandhar (India) for providing continuous support and facilities to carry out the present research.

Author contributions RR: visualization, investigation, data curation, software, formal analysis, writing original draft. NB: conceptualization, project administration, methodology, supervision, investigation, and writing—review and editing.

Funding This research did not receive any specific grant from funding agencies in the public, commercial, or not-for-profit sectors.

Declarations

Research involving human participants and/or animals No

Conflict of interest The authors declare no potential conflicts of interest concerning the research, authorship, and/or publication of this article.

References

- Arregi A, Amutio M, Lopez G, Bilbao J, Olazar M (2018) Evaluation of thermochemical routes for hydrogen production from biomass: a review. *Energy Convers Manag* 165:696–719. <https://doi.org/10.1016/j.enconman.2018.03.089>
- Li Y, Zhang Z, Zhang Q, Tahir N, Jing Y, Xia C, Zhu S, Zhang X (2020) Enhancement of bio-hydrogen yield and pH stability in photo-fermentation process using dark fermentation effluent as succedaneum. *Bioresour Technol* 297:122–504. <https://doi.org/10.1016/j.biortech.2019.122504>
- Basak N, Jana AK, Das D, Saikia D (2014) Photofermentative molecular biohydrogen production by purple-non-sulfur (PNS) bacteria in various modes: the present progress and future perspective. *Int J Hydrog Energy* 39:6853–6871. <https://doi.org/10.1016/j.ijhydene.2014.02.093>
- Zhang T, Jiang D, Zhang H, Jing Y, Tahir N, Zhang Y, Zhang Q (2020) Comparative study on bio-hydrogen production from corn stover: photo-fermentation, dark-fermentation and dark-photo co-fermentation. *Int J Hydrog Energy* 45:3807–3814. <https://doi.org/10.1016/j.ijhydene.2019.04.170>
- Phan PT, Nguyen B-S, Nguyen T-A, Kumar A, Nguyen V-H (2020) Lignocellulose-derived monosugars: a review of biomass pre-treating techniques and post-methods to produce sustainable biohydrogen. *Biomass Convers Biorefin*:1–15. <https://doi.org/10.1007/s13399-020-01161-7>
- Dębowski M, Korzeniewska E, Filipkowska Z, Zieliński M, Kwiatkowski R (2014) Possibility of hydrogen production during cheese whey fermentation process by different strains of psychrophilic bacteria. *Int J Hydrog Energy* 39:1972–1978. <https://doi.org/10.1016/j.ijhydene.2013.11.082>
- Ghimire A, Luongo V, Frunzo L, Pirozzi F, Lens PN, Esposito G (2017) Continuous biohydrogen production by thermophilic dark fermentation of cheese whey: use of buffalo manure as buffering agent. *Int J Hydrog Energy* 42:4861–4869. <https://doi.org/10.1016/j.ijhydene.2016.11.185>
- M'Arimi M, Kiprop A, Ramkat R, Kiriamiti H (2020) Progress in applications of advanced oxidation processes for promotion of biohydrogen production by fermentation processes. *Biomass Convers Biorefin*:1–25. <https://doi.org/10.1007/s13399-020-01019-y>
- Rao R, Basak N (2020) Optimization and modelling of dark fermentative hydrogen production from cheese whey by *Enterobacter aerogenes* 2822. *Int J Hydrog Energy* 46:1777–1800. <https://doi.org/10.1016/j.ijhydene.2020.10.142>
- Baeyens J, Zhang H, Nie J, Appels L, Dewil R, Ansart R, Deng Y (2020) Reviewing the potential of bio-hydrogen production by fermentation. *Renew Sust Energ Rev* 131:110023. <https://doi.org/10.1016/j.rser.2020.110023>
- Bundhoo ZM (2019) Potential of bio-hydrogen production from dark fermentation of crop residues: a review. *Int J Hydrog Energy* 44:17346–17362. <https://doi.org/10.1016/j.ijhydene.2018.11.098>
- Bao M, Su H, Tan T (2013) Dark fermentative bio-hydrogen production: effects of substrate pre-treatment and addition of metal ions or L-cysteine. *Fuel* 112:38–44. <https://doi.org/10.1016/j.fuel.2013.04.063>
- Rao R, Basak N (2020) Development of novel strategies for higher fermentative biohydrogen recovery along with novel metabolites from organic wastes: the present state of the art. *Biotechnol Appl Biochem*. <https://doi.org/10.1002/bab.1964>
- Osman AI, Deka TJ, Baruah DC, Rooney DW (2020) Critical challenges in biohydrogen production processes from the organic feedstocks. *Biomass Convers Biorefin*:1–19. <https://doi.org/10.1007/s13399-020-00965-x>
- Argun H, Kargi F (2011) Bio-hydrogen production by different operational modes of dark and photo-fermentation: an overview. *Int J Hydrog Energy* 36:7443–7459. <https://doi.org/10.1016/j.ijhydene.2011.03.116>
- Uyar B, Eroglu I, Yücel M, Gündüz U (2009) Photofermentative hydrogen production from volatile fatty acids present in dark fermentation effluents. *Int J Hydrog Energy* 34:4517–4523. <https://doi.org/10.1016/j.ijhydene.2008.07.057>
- Koku H, Eroğlu İ, Gündüz U, Yücel M, Türker L (2002) Aspects of the metabolism of hydrogen production by *Rhodobacter sphaeroides*. *Int J Hydrog Energy* 27:1315–1329. [https://doi.org/10.1016/S0360-3199\(02\)00127-1](https://doi.org/10.1016/S0360-3199(02)00127-1)
- Argun H, Kargi F (2010) Photo-fermentative hydrogen gas production from dark fermentation effluent of ground wheat solution: effects of light source and light intensity. *Int J Hydrog Energy* 35:1595–1603. <https://doi.org/10.1016/j.ijhydene.2009.12.040>
- Das SR, Basak N (2020) Molecular biohydrogen production by dark and photo fermentation from wastes containing starch: recent advancement and future perspective. *Bioprocess Biosyst Eng* 44:1–25. <https://doi.org/10.1007/s00449-020-02422-5>
- Basak N, Das D (2007) The prospect of purple non-sulfur (PNS) photosynthetic bacteria for hydrogen production: the present state of the art. *World J Microbiol Biotechnol* 23:31–42. <https://doi.org/10.1007/s11274-006-9190-9>
- Hitam C, Jalil A (2020) A review on biohydrogen production through photo-fermentation of lignocellulosic biomass. *Biomass Convers Biorefin*:1–19. <https://doi.org/10.1007/s13399-020-01140-y>

22. Sybounya S, Nitisravut R (2020) Hybrid composite of modified commercial activated carbon and Zn-Ni hydrotalcite for fermentative hydrogen production. *J Environ Chem Eng*:104801. <https://doi.org/10.1016/j.jece.2020.104801>
23. Castillo-Moreno P, Serrato JC, Willison JC, Magnin J-P (2018) Photohydrogen production from lactose and lactate by recombinant strains of *Rhodobacter capsulatus*: modeling and optimization. *Int J Hydrog Energy* 43:21231–21245. <https://doi.org/10.1016/j.ijhydene.2018.09.038>
24. Dolly S, Pandey A, Pandey BK, Gopal R (2015) Process parameter optimization and enhancement of photo-biohydrogen production by mixed culture of *Rhodobacter sphaeroides* NMBL-02 and *Escherichia coli* NMBL-04 using Fe-nanoparticle. *Int J Hydrog Energy* 40:16010–16020. <https://doi.org/10.1016/j.ijhydene.2015.09.089>
25. Laocharoen S, Reungsang A (2014) Isolation, characterization and optimization of photo-hydrogen production conditions by newly isolated *Rhodobacter sphaeroides* KKU-PS5. *Int J Hydrog Energy* 39:10870–10882. <https://doi.org/10.1016/j.ijhydene.2014.05.055>
26. Li Y, Zhang Z, Jing Y, Ge X, Wang Y, Lu C, Zhou X, Zhang Q (2017) Statistical optimization of simultaneous saccharification fermentative hydrogen production from *Platanus orientalis* leaves by photosynthetic bacteria HAU-M1. *Int J Hydrog Energy* 42:5804–5811. <https://doi.org/10.1016/j.ijhydene.2016.11.182>
27. Liu H, Zhang Z, Zhang Q, Tahir N, Jing Y, Li Y, Lu C (2019) Optimization of photo fermentation in corn stalk through phosphate additive. *Bioresour Technol Rep* 7:100278. <https://doi.org/10.1016/j.biteb.2019.100278>
28. Valentin JD, Qin X-H, Fessele C, Straub H, van der Mei HC, Buhmann MT, Maniura-Weber K, Ren Q (2019) Substrate viscosity plays an important role in bacterial adhesion under fluid flow. *J Colloid Interface Sci* 552:247–257. <https://doi.org/10.1016/j.jcis.2019.05.043>
29. Asunis F, De Gioannis G, Isipato M, Muntoni A, Poletini A, Pomi R, Rossi A, Spiga D (2019) Control of fermentation duration and pH to orient biochemicals and biofuels production from cheese whey. *Bioresour Technol* 289:121722. <https://doi.org/10.1016/j.biortech.2019.121722>
30. Chandrasekhar K, Lee Y-J, Lee D-W (2015) Biohydrogen production: strategies to improve process efficiency through microbial routes. *Int J Mol Sci* 16:8266–8293. <https://doi.org/10.3390/ijms16048266>
31. Özgür E, Uyar B, Öztürk Y, Yücel M, Gündüz U, Eroğlu I (2010) Biohydrogen production by *Rhodobacter capsulatus* on acetate at fluctuating temperatures. *Resour Conserv Recycl* 54:310–314. <https://doi.org/10.1016/j.resconrec.2009.06.002>
32. Lazaro CZ, Varesche MBA, Silva EL (2015) Effect of inoculum concentration, pH, light intensity and lighting regime on hydrogen production by phototrophic microbial consortium. *Renew Energy* 75:1–7. <https://doi.org/10.1016/j.renene.2014.09.034>
33. Basak N, Jana AK, Das D (2014) Optimization of molecular hydrogen production by *Rhodobacter sphaeroides* OU 001 in the annular photobioreactor using response surface methodology. *Int J Hydrog Energy* 39:11889–11901. <https://doi.org/10.1016/j.ijhydene.2014.05.108>
34. Androga DD, Sevinç P, Koku H, Yücel M, Gündüz U, Eroglu I (2014) Optimization of temperature and light intensity for improved photofermentative hydrogen production using *Rhodobacter capsulatus* DSM 1710. *Int J Hydrog Energy* 39:2472–2480. <https://doi.org/10.1016/j.ijhydene.2013.11.114>
35. Al-Mohammedawi HH, Znad H, Eroglu E (2018) Synergistic effects and optimization of photo-fermentative hydrogen production of *Rhodobacter sphaeroides* DSM 158. *Int J Hydrog Energy* 43:15823–15834. <https://doi.org/10.1016/j.ijhydene.2018.06.140>
36. Shi X-Y, Li W-W, Yu H-Q (2014) Optimization of H₂ photo-fermentation from benzoate by *Rhodospseudomonas palustris* using a desirability function approach. *Int J Hydrog Energy* 39:4244–4251. <https://doi.org/10.1016/j.ijhydene.2014.01.016>
37. Mishra P, Singh L, Ab Wahid Z, Krishnan S, Rana S, Islam MA, Sakinah M, Ameen F, Syed A (2018) Photohydrogen production from dark-fermented palm oil mill effluent (DPOME) and statistical optimization: renewable substrate for hydrogen. *J Clean Prod* 199:11–17. <https://doi.org/10.1016/j.jclepro.2018.07.028>
38. Wang R, Wen H, Cui C (2019) Bio-hydrogen production by a new isolated strain *Rhodospseudomonas* sp. WR-17 using main metabolites of three typical dark fermentation type. *Int J Hydrog Energy* 44:25145–25150. <https://doi.org/10.1016/j.ijhydene.2019.04.143>
39. Lin R, Cheng J, Yang Z, Ding L, Zhang J, Zhou J, Cen K (2016) Enhanced energy recovery from cassava ethanol wastewater through sequential dark hydrogen, photo hydrogen and methane fermentation combined with ammonium removal. *Bioresour Technol* 214:686–691. <https://doi.org/10.1016/j.biortech.2016.05.037>
40. Nasr M, Tawfik A, Ookawara S, Suzuki M, Kumari S, Bux F (2015) Continuous biohydrogen production from starch wastewater via sequential dark-photo fermentation with emphasize on maghemite nanoparticles. *J Ind Eng Chem* 21:500–506. <https://doi.org/10.1016/j.jiec.2014.03.011>
41. Moreno R, Escapa A, Cara J, Carracedo B, Gómez X (2015) A two-stage process for hydrogen production from cheese whey: integration of dark fermentation and biocatalyzed electrolysis. *Int J Hydrog Energy* 40:168–175. <https://doi.org/10.1016/j.ijhydene.2014.10.120>
42. Rai PK, Singh S, Asthana R (2012) Biohydrogen production from cheese whey wastewater in a two-step anaerobic process. *Appl Biochem Biotechnol* 167:1540–1549. <https://doi.org/10.1007/s12010-011-9488-4>
43. Alvarez-Guzmán CL, Cisneros-de la Cueva S, Balderas-Hernández VE, Smoliński A, De León-Rodríguez A (2020) Biohydrogen production from cheese whey powder by *Enterobacter asburiae*: effect of operating conditions on hydrogen yield and chemometric study of the fermentative metabolites. *Energy Rep* 6:1170–1180. <https://doi.org/10.1016/j.egy.2020.04.038>
44. Seifert K, Waligorska M, Laniecki M (2010) Hydrogen generation in photobiological process from dairy wastewater. *Int J Hydrog Energy* 35:9624–9629
45. Rai PK, Asthana R, Singh S (2014) Optimization of photo-hydrogen production based on cheese whey spent medium. *Int J Hydrog Energy* 39:7597–7603. <https://doi.org/10.1016/j.ijhydene.2013.09.011>
46. Fang F, Mu Y, Sheng G-P, Yu H-Q, Li Y-Y, Kubota K, Harada H (2013) Kinetic analysis on gaseous and aqueous product formation by mixed anaerobic hydrogen-producing cultures. *Int J Hydrog Energy* 38:15590–15597. <https://doi.org/10.1016/j.ijhydene.2013.03.157>
47. Nath K, Das D (2011) Modeling and optimization of fermentative hydrogen production. *Bioresour Technol* 102:8569–8581. <https://doi.org/10.1016/j.biortech.2011.03.108>
48. Rasdi Z, Mumtaz T, Hassan MA (2012) Kinetic analysis of biohydrogen production from anaerobically treated POME in bioreactor under optimized condition. *Int J Hydrog Energy* 37:17724–17730. <https://doi.org/10.1016/j.ijhydene.2012.08.095>
49. Blanco V, Oliveira G, Zaiat M (2019) Dark fermentative biohydrogen production from synthetic cheese whey in an anaerobic structured-bed reactor: performance evaluation and kinetic modeling. *Renew Energy* 139:1310–1319. <https://doi.org/10.1016/j.renene.2019.03.029>
50. Sharma Y, Li B (2009) Optimizing hydrogen production from organic wastewater treatment in batch reactors through experimental

- and kinetic analysis. *Int J Hydrog Energy* 34:6171–6180. <https://doi.org/10.1016/j.ijhydene.2009.06.031>
51. Koku H, Eroglu I, Gunduz U, Yücel M, Türker L (2003) Kinetics of biological hydrogen production by the photosynthetic bacterium *Rhodobacter sphaeroides* OU 001. *Int J Hydrog Energy* 28:381–388. [https://doi.org/10.1016/S0360-3199\(02\)00080-0](https://doi.org/10.1016/S0360-3199(02)00080-0)
 52. Biebl H, Pfenig N (1981) Isolation of members of the family *Rhodospirillaceae*. The prokaryotes Springer, Isolation of Members of the Family Rhodospirillaceae
 53. Basak N, Jana AK, Das D (2016) CFD modeling of hydrodynamics and optimization of photofermentative hydrogen production by *Rhodopseudomonas palustris* DSM 123 in annular photobioreactor. *Int J Hydrog Energy* 41:7301–7317. <https://doi.org/10.1016/j.ijhydene.2016.02.126>
 54. Nath K, Muthukumar M, Kumar A, Das D (2008) Kinetics of two-stage fermentation process for the production of hydrogen. *Int J Hydrog Energy* 33:1195–1203. <https://doi.org/10.1016/j.ijhydene.2007.12.011>
 55. Don MM, Shoparwe NF (2010) Kinetics of hyaluronic acid production by *Streptococcus zooepidemicus* considering the effect of glucose. *Biochem Eng J* 49:95–103. <https://doi.org/10.1016/j.bej.2009.12.001>
 56. Luedeking R, Piret EL (1959) A kinetic study of the lactic acid fermentation. Batch process at controlled pH. *J Biochem Microbiol Technol Eng* 1:393–412. <https://doi.org/10.1002/jbmt.390010406>
 57. Sangyoka S, Reungsang A, Lin C-Y (2016) Optimization of biohydrogen production from sugarcane bagasse by mixed cultures using a statistical method. *Sustain Environ Res* 26:235–242. <https://doi.org/10.1016/j.serj.2016.05.001>
 58. Saraphirom P, Reungsang A (2010) Optimization of biohydrogen production from sweet sorghum syrup using statistical methods. *Int J Hydrog Energy* 35:13435–13444. <https://doi.org/10.1016/j.ijhydene.2009.11.122>
 59. Lu C, Zhang Z, Zhou X, Hu J, Ge X, Xia C, Zhao J, Wang Y, Jing Y, Li Y (2018) Effect of substrate concentration on hydrogen production by photo-fermentation in the pilot-scale baffled bioreactor. *Bioresour Technol* 247:1173–1176. <https://doi.org/10.1016/j.biortech.2017.07.122>
 60. Ghosh D, Sobro IF, Hallenbeck PC (2012) Optimization of the hydrogen yield from single-stage photofermentation of glucose by *Rhodobacter capsulatus* JP91 using response surface methodology. *Bioresour Technol* 123:199–206. <https://doi.org/10.1016/j.biortech.2012.07.061>
 61. Hitit ZY, Lazaro CZ, Hallenbeck PC (2017) Hydrogen production by co-cultures of *Clostridium butyricum* and *Rhodospseudomonas palustris*: optimization of yield using response surface methodology. *Int J Hydrog Energy* 42:6578–6589. <https://doi.org/10.1016/j.ijhydene.2016.12.122>
 62. Sun Q, Xiao W, Xi D, Shi J, Yan X, Zhou Z (2010) Statistical optimization of biohydrogen production from sucrose by a co-culture of *Clostridium acidisoli* and *Rhodobacter sphaeroides*. *Int J Hydrog Energy* 35:4076–4084. <https://doi.org/10.1016/j.ijhydene.2010.01.145>
 63. Hassan N, Jalil A, Vo D, Nabgan W (2020) An overview on the efficiency of biohydrogen production from cellulose. *Biomass Convers Biorefin*:1–23. <https://doi.org/10.1007/s13399-020-01125-x>
 64. Chen C-Y, Lu W-B, Wu J-F, Chang J-S (2007) Enhancing phototrophic hydrogen production of *Rhodopseudomonas palustris* via statistical experimental design. *Int J Hydrog Energy* 32:940–949. <https://doi.org/10.1016/j.ijhydene.2006.09.021>
 65. Dasgupta CN, Gilbert JJ, Lindblad P, Heidom T, Borgvang SA, Skjanes K, Das D (2010) Recent trends on the development of photobiological processes and photobioreactors for the improvement of hydrogen production. *Int J Hydrog Energy* 35:10218–10238. <https://doi.org/10.1016/j.ijhydene.2010.06.029>
 66. Tiang MF, Hanipa MAF, Abdul PM, Jahim JM, Mahmud SS, Takriff MS, Lay C-H, Reungsang A, Wu S-Y (2020) Recent advanced biotechnological strategies to enhance photo-fermentative biohydrogen production by purple non-sulphur bacteria: an overview. *Int J Hydrog Energy*:13211–13230. <https://doi.org/10.1016/j.ijhydene.2020.03.033>
 67. Garimella S, Vimal A, Merugu R, Kumar A (2019) Optimization for enhanced hydrogen production from *Rhodobacter sphaeroides* using response surface methodology. *SN Appl Sci* 1:156
 68. Mishra P, Ab Wahid Z, Zaid RM, Rana S, Tabassum S, Karim A, Singh L, Islam MA, Jaing X, Sakinah M (2020) Kinetics and statistical optimization study of bio-hydrogen production using the immobilized photo-bacterium. *Biomass Convers Biorefin*:1–12. <https://doi.org/10.1007/s13399-020-00835-6>
 69. Özgen C (2011) Microarray analysis of the effects of heat and cold stress on hydrogen production metabolism of *Rhodobacter capsulatus*. Citeseer
 70. Phadtare S (2004) Recent developments in bacterial cold-shock response. *Curr Issues Mol Biol* 6:125–136
 71. Chen W-H, Chen S-Y, Khanal SK, Sung S (2006) Kinetic study of biological hydrogen production by anaerobic fermentation. *Int J Hydrog Energy* 31:2170–2178. <https://doi.org/10.1016/j.ijhydene.2006.02.020>
 72. Chen C-Y, Yeh K-L, Lo Y-C, Wang H-M, Chang J-S (2010) Engineering strategies for the enhanced photo-H₂ production using effluents of dark fermentation processes as substrate. *Int J Hydrog Energy* 35:13356–13364. <https://doi.org/10.1016/j.ijhydene.2009.11.070>
 73. Han H, Liu B, Yang H, Shen J (2012) Effect of carbon sources on the photobiological production of hydrogen using *Rhodobacter sphaeroides* RV. *Int J Hydrog Energy* 37:12167–12174. <https://doi.org/10.1016/j.ijhydene.2012.03.134>
 74. Mullai P, Rene ER (2013) Sridevi K (2013) Biohydrogen production and kinetic modeling using sediment microorganisms of pichavaram mangroves, India. *Biomed Res Int* 2013:1–9. <https://doi.org/10.1155/2013/265618>
 75. Gadhe A, Sonawane SS, Varma MN (2014) Kinetic analysis of biohydrogen production from complex dairy wastewater under optimized condition. *Int J Hydrog Energy* 39:1306–1314
 76. Hu B, Li Y, Zhu S, Zhang H, Jing Y, Jiang D, He C, Zhang Z (2020) Evaluation of biohydrogen yield potential and electron balance in the photo-fermentation process with different initial pH from starch agricultural leftover. *Bioresour Technol*:122900. <https://doi.org/10.1016/j.biortech.2020.122900>
 77. Shi XY, Yu HQ (2005) Optimization of glutamate concentration and pH for H₂ production from volatile fatty acids by *Rhodopseudomonas capsulata*. *Lett Appl Microbiol* 40:401–406. <https://doi.org/10.1111/j.1472-765X.2005.01700.x>
 78. Uyar B, Eroglu I, Yücel M, Gunduz U, Türker L (2007) Effect of light intensity, wavelength and illumination protocol on hydrogen production in photobioreactors. *Int J Hydrog Energy* 32:4670–4677. <https://doi.org/10.1016/j.ijhydene.2007.07.002>
 79. Basak N, Das D (2009) Photofermentative hydrogen production using purple non-sulfur bacteria *Rhodobacter sphaeroides* OU 001 in an annular photobioreactor: a case study. *Biomass Bioenergy* 33:911–919. <https://doi.org/10.1016/j.biombioe.2009.02.007>
 80. Adessi A, McKinlay JB, Harwood CS, De Philippis R (2012) A *Rhodopseudomonas palustris* nifA* mutant produces H₂ from NH₄⁺-containing vegetable wastes. *Int J Hydrog Energy* 37:15893–15900
 81. Zagrodnik R, Thiel M, Seifert K, Włodarczak M, Łaniecki M (2013) Application of immobilized *Rhodobacter sphaeroides* bacteria in hydrogen generation process under semi-continuous

- conditions. *Int J Hydrog Energy* 38:7632–7639. <https://doi.org/10.1016/j.ijhydene.2010.07.015>
82. Cardena R, Moreno G, Valdez-Vazquez I, Buitrón G (2015) Optimization of volatile fatty acids concentration for photofermentative hydrogen production by a consortium. *Int J Hydrog Energy* 40:17212–17223. <https://doi.org/10.1016/j.ijhydene.2015.10.020>
83. Corneli E, Adessi A, Dragoni F, Ragaglini G, Bonari E, De Philippis R (2016) Agroindustrial residues and energy crops for the production of hydrogen and poly- β -hydroxybutyrate via photofermentation. *Bioresour Technol* 216:941–947. <https://doi.org/10.1016/j.biortech.2016.06.046>
84. Silva FTM, Moreira LR, de Souza FJ, Batista FRX, Cardoso VL (2016) Replacement of sugars to hydrogen production by *Rhodobacter capsulatus* using dark fermentation effluent as substrate. *Bioresour Technol* 200:72–80. <https://doi.org/10.1016/j.biortech.2015.10.002>
85. Krujatz F, Härtel P, Helbig K, Haufe N, Thierfelder S, Bley T, Weber J (2015) Hydrogen production by *Rhodobacter sphaeroides* DSM 158 under intense irradiation. *Bioresour Technol* 175:82–90. <https://doi.org/10.1016/j.biortech.2014.10.061>
86. Li X, Dai Z-Z, Wang Y-H, Zhang S-L (2011) Enhancement of phototrophic hydrogen production by *Rhodobacter sphaeroides* ZX-5 using fed-batch operation based on ORP level. *Int J Hydrog Energy* 36:12794–12802. <https://doi.org/10.1016/j.ijhydene.2011.07.070>

Publisher's note Springer Nature remains neutral with regard to jurisdictional claims in published maps and institutional affiliations.